Accepted Manuscript

Precipitates in metals that dissolve on cooling and form on heating: An example with hydrogen in alpha-zirconium

G.A. McRae, C.E. Coleman

PII: S0022-3115(16)30529-3

DOI: 10.1016/j.jnucmat.2017.09.017

Reference: NUMA 50503

To appear in: *Journal of Nuclear Materials*

Received Date: 2 August 2016

Revised Date: 11 September 2017

Accepted Date: 13 September 2017

Please cite this article as: G.A. McRae, C.E. Coleman, Precipitates in metals that dissolve on cooling and form on heating: An example with hydrogen in alpha-zirconium, *Journal of Nuclear Materials* (2017), doi: 10.1016/j.jnucmat.2017.09.017.

Precipitates in metals that dissolve on cooling and form on heating: an example with hydrogen in alpha-zirconium

G.A. McRae[1] and C.E. Coleman[2]

[1]Carleton University, Ottawa, Canada

[2]Canadian Nuclear Laboratories, Chalk River, Ontario, Canada.

Abstract

Einstein's theory for Brownian motion and Gibbs' Phase Rule along with diffraction of high intensity X-rays have been used to provide an interpretation of precipitation and dissolution in metals using hydrides in alpha-zirconium as an example. Hydrides precipitated, and dissolved during cooling, and at some temperatures, their amounts increased with heating. Hydrides were seen to precipitate without exothermic signals both above and below the solvus temperature, and on heating, were found to be stable above the solvus temperature. Hydrides were inferred to form composites with the delta phase surrounded by gamma phase. These results are interpreted with Cottrell atmospheres of hydrogen atoms that relieve the stress around dislocations, and hydrogen clouds from stresses around hydrides making them stable against dissolution leading to maxima in the amounts of hydrides with change in temperature. A vertical line corresponding to ZrH is suggested to be added to the equilibrium phase diagram to comply with the Phase Rule.

Keywords: precipitation; dissolution; diffraction; hydrides; zirconium; Cottrell atmospheres, hydrogen clouds, elastic stress concentration factor

Precipitates in metals that dissolve on cooling and form on heating: an example with hydrogen in alpha-zirconium

Introduction:

It is everyday experience that solutes precipitating from liquid solutions at constant pressure form in ever increasing amounts as the temperature is lowered. When the temperature is increased, these precipitates dissolve. At low temperatures, the entropy contribution to the free energy, $-T\Delta S$, is small compared with the enthalpy of formation of the precipitate, whereas at higher temperatures the entropy contribution favours a well-dispersed solute. The temperature where the switch occurs between precipitation and dissolution is called the solvus temperature. In this simple two-component two-phase constant-pressure liquid-solvent example, precipitation increases with cooling and precipitates dissolve with heating.

When the solvent is a solid, the equivalent of pressure for liquids is hydrostatic stress, which is no longer constant: there will always be internal defects, for example, dislocations, that give rise to local gradients in hydrostatic stress seen by the solute. Applied stresses can lead to hydrostatic stress gradients in the solvent. Both stress gradients allow precipitates to form and dissolve above and below the solvus temperature.

Our example is hydrogen in zirconium. Hydrogen atoms move interstitially in solid solution and increase the lattice parameters of the zirconium. Hydrides also expand the lattice locally, which results in regions of tensile stress in the zirconium and compression in the hydride.

There are two hydride phases commonly seen in zirconium. These phases are the δ-phase, with stoichiometry reported between $ZrH_{1.5}$ (Zr_2H_3) and $ZrH_{1.67}$ (Zr_3H_5), and the γ-phase, ZrH [1]. The δ-phase, with a calculated formation energy between -53 and -57 kJ/mol atom, might be expected to be more stable than the γ-phase, with a formation energy of -31 to -49 kJ/mol atom [2, 3], but when entropy is included, the free energy suggests that the γ-phase will be the more stable, although the free energy of the two phases is very close [4]. The γ-phase forms as long needles, and the δ-phase forms crystals that are platelets [5], both having sharp edges that may act as local stress concentrators.

Gibbs' Phase Rule [6] is tested by the simultaneous observation of γ-phase and δ-phase in α-zirconium: hydrogen in solution in the metal cannot simultaneously be in equilibrium with two hydride phases. Gibbs' Phase Rule relates the number of components, *C*, and the number of phases in equilibrium in gradient-free solids, *P*, to the number of degrees of freedom, *F*, that are independent intensive variables that can completely describe the system thermodynamically through:

$$F = C - P + 1 \quad (1)$$

Hydrogen and zirconium are the two components, so C=2. For a single hydride phase and hydrogen in solution at equilibrium, there are two phases, so P=2 and F=1. There is one degree of freedom. For phase diagrams written in terms of the intensive variables concentration and temperature, the Phase Rule says that only one of these variables is independent. Thus, if temperature is chosen to describe the system, the concentration is given by a unique value on the phase boundary curve and vice versa. But, if γ-phase, and δ-phase exist independently and simultaneously with hydrogen in solution at equilibrium, then P=3, and F=0, there are no degrees of freedom. In this case, there could be no variation of the equilibrium with an intensive variable such as temperature or concentration, which is not observed – the phase diagram for the

solvus shows unique equilibria happen for concentrations that depend on temperatures, or vice versa.

Equilibrium between hydrogen in solution and hydrogen as hydride is dynamic: hydrogen in solution in the zirconium matrix leaves solution to precipitate as hydride, and hydrogen in hydrides leaves the hydrides to go into solution, the rates for these processes are equal and opposite at equilibrium. For hydrogen in solid solution (SS) in equilibrium with hydride in zirconium:

$$\text{Hydride} \rightleftharpoons \text{Zr} + \text{H}_{(SS)} \quad (2)$$

The concentration of hydrogen in solution in the metal volume adjacent to hydrides defines the solvus concentration.

This paper presents X-ray diffraction data showing isothermal measurements of hydrogen concentration in solution in zirconium, and the formation of γ-phase and δ-phase hydrides, during heating and cooling. Comparisons will be made with heat flow determined using Differential Scanning Calorimetry (DSC). The experimental results in this paper will be used to test predictions made with the flux relation developed by Einstein for Brownian motion [7], and previously used to predict delayed hydride cracking rates [8]. The results are different from other applications of the Einstein flux because a solvus is crossed.

The focus of this paper is on precipitates dissolving during cooling and forming during heating. The experimental results presented here also provide additional observations of the relationship between γ-hydrides and δ-hydrides in zirconium at low hydrogen concentrations and temperatures, and suggest an interpretation of the apparent hysteresis observed between the temperatures at which hydrides precipitate and dissolve.

Background

Observations of γ- and δ-hydrides in zirconium

The phases of the zirconium-hydrogen system are controversial. Much of the reported variation in the presence of each hydride phase is caused by comparing materials with a range of concentrations of hydrogen, impurity and alloying elements, after various cooling rates and hold times at different temperatures, various grain structures of the zirconium alloy, and different temperatures of examination. The studies of the stability of the γ-phase have yielded conflicting results with different explanations as the following examples demonstrate.

In some studies low hydrogen concentrations, < 1.3 at.% (140 ppm), favoured the formation of γ-hydride [9, 10, 11] in pure zirconium and in Zircaloy-4 [12]. In [10] above 0.89 at.% (98 ppm) hydrogen, a mixture of δ-hydrides and γ-hydrides was observed, while below 0.19 at.% (21 ppm) hydrogen, only γ-hydride could be detected. To test the stability of the hydride phases, specimens with hydrogen concentrations of 0.19 at.% (21 ppm) and 0.89 at.% (98 ppm) were heated to 200 °C for two weeks and furnace-cooled. Only γ-hydrides were observed, indicating that the γ-phase had not transformed to the δ-phase but vice versa. Most of the hydrides were precipitated within the grains since in this test material the grain size was 500 μm whereas in [13], the grain size was about ten times smaller thus providing a large area of grain boundaries, where δ-hydride was found. In [11], the specimens were re-examined after three years at room temperature and the γ-hydride had not converted to δ-hydride.

Precipitates in metals that dissolve on cooling and form on heating: an example with hydrogen in alpha-zirconium

The elastic strain energies of the γ- and δ-hydrides were estimated to be 6.9 kJ/mol and 8.4 kJ/mol, respectively, implying that the γ-phase is expected to nucleate first from solid solution [14]. If stress-relieving accommodation dislocations are formed around the precipitates, the total strain energy declines and depends on the yield strength of the material [15]. With low strength material, ratio of yield strength/shear modulus, σ_y/μ, of 0.001, the strain energies for each hydride phase are small, <0.45 kJ/mol, and about the same size so that once γ-hydride is nucleated it continues to grow [14]. In material with high strength, σ_y/μ, of 0.01, the strain energies increase but for δ-hydride the energy required is slightly smaller than for γ-hydride, 2.4 kJ/mol to 2.5 kJ/mol. The analysis assumed an absence of any significant difference in chemical formation energy. Thus after slow cooling the δ-hydride was the expected phase in strong materials, except when the hydrogen concentration was less than 100 ppm. This analysis was used to explain the presence of γ-phase in zirconium with low oxygen concentration and δ-phase when oxygen was added to the same material [14].

In Zircaloy-2 with about 0.90 at.% (100 ppm) hydrogen in solution, the formation of γ-hydride by fast quenching was suppressed by increasing the strength by cold-work [16]. An alternative explanation to the local difference in volume expansion for the effect of strength is that for a given concentration of hydrogen, the lower H/Zr required by γ-hydride compared with δ-hydride provides a higher number density of precipitates, $N_f^\gamma > N_f^\delta$, therefore the total strain required is greater for γ-hydride than δ-hydride. If only γ-hydride formed, the total strain, ε_T^γ, would be (N_f^γ x 0.123), whereas if only δ-hydride formed, the total strain, ε_T^δ, would be (N_f^δ x 0.172/1.6), that is, N_f^δ x 0.108, so $\varepsilon_T^\gamma > \varepsilon_T^\delta$, thus explaining the effect of strength. If hydride nucleation at dislocations from cold-work was the controlling process, precipitation of γ-hydride would be promoted but such an increase was not observed.

- When the cooling rate was varied from brine quenching to furnace cooling, the strength effect was not observed in Zr-2.5Nb [17, 16] when the β-phase was present, which provides hydride nucleation at α/β interfaces [18, 19]. With low concentrations of hydrogen, 0.06 at.% (7 ppm), only γ-hydride was precipitated, even with furnace cooling; with a moderate concentration, 0.42 at.% (46 ppm), γ-hydride was still observed with oil quenching but δ-hydride was detected after air cooling; a mixture of γ- and δ-hydrides was found after all coolings when the hydrogen concentration was 1.3 at.% (140 ppm); only δ-phase was observed with air cooling and furnace cooling with a hydrogen concentration of 2.7 at.% (300 ppm).
- With hydrogen concentrations of 1.8 at.% (200 ppm) and 4.4 at.% (500 ppm) in pure Zr, γ-hydrides from water quenching transformed almost completely to δ-hydride after aging at 200 °C for 3 weeks. Aging at 150 °C only partially converted the γ-hydride to δ-hydride after 3 weeks. After furnace cooling from the solution temperature only δ-hydrides were detected and these precipitates did not change with aging [20].
- Lanzani and Ruch [21] added between 1.56 at.% (174 ppm) and 12.15 at.% (1514 ppm) hydrogen to Zircaloy-4 by corrosion then subjected specimens to storage at room temperature for various hold times totalling 37 months, with an intermediate heating to 148 °C for 2212 h. No γ-phase was detected by X-ray diffraction.
- Synchrotron evaluations at room temperature of Zircaloy containing up to 21.5 at.% (3000 ppm) hydrogen revealed mostly δ-hydrides, with traces of γ-hydride. ε-hydride

was detected in hydride layers containing about 35 at.% (6 000 ppm) hydrogen on the rim of cladding [22, 23].

- Specimens of pure Zr containing up to 60 at.% (16 000 ppm) contained a mixture of γ- and δ-hydrides after cooling from the β-phase [24]. After furnace cooling the δ-hydride dominated whereas after water quenching γ-hydride was prominent. After aging for 6.5 months at room temperature, in the water-quench materials, the volume of the γ-hydride increased at the expense of the δ-hydride and approached ZrH at 50 at.% (11 000 ppm) hydrogen. The stability of the γ-phase at room temperature was indicated by the decoration of δ-hydride with γ-hydride in pure Zr containing 55.5 at.% (13 500 ppm) hydrogen after holding for 174 days following a furnace cool from 500°C [25]; γ-hydride in the matrix remained unchanged.
- With high concentrations of hydrogen, 48 at.% to 60 at.% (10 000 ppm to 16 000 ppm), the material mostly consisted of a mixture of γ-hydride and δ-hydride [24, 26, 27]. Heating to over 250 °C (523 K) converted all the γ-hydride to δ-hydride.
- In Zircaloy-2 containing 0.9 at.% (100 ppm) hydrogen, electron energy loss spectroscopy showed that the composition of a hydride could vary from ZrH at the tip to $ZrH_{1.7}$ in the core of the hydride [28].
- No γ-hydride was observed in specimens of Zr-1.15Cr-0.1Fe containing 27.7 at.% (4200 ppm) hydrogen [29]; heating for 2200 h at 220 °C – 20 °C below a suspected transformation temperature – yielded no γ-hydride.

Studies of hydrogen in annealed Zircaloy using diffraction of X-rays from a synchrotron have used the δ-phase to represent hydrides during temperature cycling [30, 31, 32]. These experiments explored the solubility limits of hydrogen in Zr, the kinetics of hydride nucleation and growth and the crystallographic features of reoriented hydrides. The common features of the experiments are large hydrogen concentrations, 0.72 at.% to 5.2 at.% (80 ppm to 600 ppm), and continuous temperature changes between 5 °C/s and around 10 °C/minute.

Neutron diffraction measurements have shown that the γ-phase is the stable hydride at room temperature in the strong alloy Zr-2.5Nb. During heating of a specimen containing 0.783 at.% (87 ppm) hydrogen isotopes, about 60% of the γ-phase signal was lost and δ-phase formed at about 180 ºC [33]. During cooling from well above this temperature the first phase detected was δ-hydride. The formation of γ-hydride at room temperature was slow, with a characteristic time scale of the order of months [34, 35]. As shown for hydrides in pure Zr [25], the γ-hydride consumed the δ-hydride precipitate from outside-in, and after a further year of storage only a small island of δ-hydride remains [35], Figure 1.

Although most phase diagrams omit the γ-phase, preferring to consider it a metastable phase, some of the above results and observations suggest there is a transformation to γ-hydride at low temperatures within the phase field between the α/(α+δ) and (α+δ)/δ boundaries with a transformation temperature between 180 °C to 250 °C. Two studies showed that a difference in strength could affect which hydride formed, either because their plastic strain energies were similar [14] or because their composition determined their number density [16]. Atomic-scale calculations of the properties of the Zr–H system [36, 37] indicate that the formation energies of the hydrides are about 5 to 15 times larger than the strain energies and the difference between the formation energies of γ- and δ-hydrides is 15% and 25%, with δ-hydrides being the more stable. These results suggest that because of the modest differences between each of the contributions to

the energies of the precipitation of the two hydrides, when embedded within the zirconium matrix their relative stabilities may depend on mechanical and thermal contributions to their free energies, modified by slight variations in composition and fabrication of the component. Whether γ-hydride or δ-hydride or both are present in a material depends on the hydrogen concentration, zirconium alloy composition and the thermomechanical treatments, and time at the low temperature.

Terminal Solid Solubility

An alternative interpretation of 'Terminal Solid Solubility' (TSS) is presented in this paper. TSS refers to the equilibrium phase boundary between hydrogen in solution in the metal, and hydrogen in hydride. This equilibrium phase boundary is known as the solvus. In the standard interpretation, this phase boundary is not unique because it depends on whether it is approached by heating or cooling. Hence, 'equilibrium', in the standard interpretation of the solvus, is meant in a 'restricted and dynamic' sense depending on whether the sample is heated or cooled: the solvus where hydrides precipitate upon cooling is labeled TSSP, and the solvus where hydrides dissolve upon heating is labeled TSSD.

The cooling-heating cycle often used to explain the standard interpretation is shown in Figure 2 along with representative TSSP (upper) and TSSD (lower) curves. The cooling-heating cycle starts at Point A where all of the hydrogen is in solution (*i.e.*, Point A is below the TSSD concentration and above the TSSD temperature). For this example, the total hydrogen concentration is 1 at.% (110 ppm) and the starting temperature is 360 ^{o}C. As the alloy is cooled, the hydrogen concentration in solution remains at 1 at.% (110 ppm) until Point B is reached. During cooling from Point A to Point B, there is no observable effect of crossing the TSSD line - the TSSD line is not apparent during cooling. Upon further cooling, hydrides can nucleate. Once hydrides form, the concentration of hydrogen in solution follows the TSSP line as the alloy is cooled to Point C. In the heating portion of the cycle, the alloy is first heated from Point C to Point D. During heating the TSSP line is not apparent, but now the TSSD line is. On heating, the solvus line is given by TSSD. Between Points C and D, the temperatures are below the TSSD temperature and, hence, the concentration of hydrogen in solution does not change until Point D, which is where the horizontal line between Points C and D intersects with the TSSD curve. At Point D, the hydrides begin to dissolve with further heating, and the hydrogen concentration in solution follows the TSSD line until Point E, which is where all the hydrides have dissolved and where the concentration in solution is again 1 at.% (110 ppm). The concentration of hydrogen in solution stays at 1 at.% (110 ppm) as the temperature is raised to the starting value.

The standard interpretation is that the hydrogen concentration in solution is the lesser of [38, 39]:

- The total hydrogen content;
- The composition of the solvus for hydride dissolution during heating;
- The composition of the solvus for hydride precipitation during cooling.

In addition, when switching between cooling and heating there is a hiatus where the concentration does not change because of a hysteresis [40], *i.e.*, the horizontal line between Points C and D in Figure 2.

Precipitates in metals that dissolve on cooling and form on heating: an example with hydrogen in alpha-zirconium

In the standard interpretation, both TSSP and TSSD are solvus lines, and both represent equilibrium conditions, albeit in the 'restricted sense' of while the temperature is changing - cooling for TSSP and heating for TSSD. These solvus lines do not exist at the same time, because you cannot cool and heat simultaneously, but they do exist at the same location. During heating, all locations within the alloy see TSSD as the solvus, and during cooling all locations see TSSP as the solvus. The shift of the solvus between TSSP and TSSD is called the hysteresis [40], which is interpreted to mean that the concentration of hydrogen in solution for hydride dissolution is less than for hydride precipitation, or, equivalently, the temperature for hydride dissolution is greater than for hydride formation. The temperature hysteresis between hydride precipitation, given by TSSP, and dissolution, given by TSSD, can be as large as 60 ^{o}C for the same concentration, depending on which features of the experimental measurements are used to indicate precipitation and dissolution.

For thermodynamic equilibrium, according to the Phase Rule, composition and temperature cannot be changed independently for two phases to be present in a binary alloy. At the same composition, hydrides should dissolve and precipitate at the same temperature independent of heating or cooling. The presence of two values of the solubility limit suggests that one or both the values do not represent equilibrium and the hysteresis and values are therefore indicated as "apparent". In dynamic measurements, values of apparent TSS by heating or cooling are clearly distinguishable and reproducible even if strictly invalid as equilibrium values. They are of practical use for evaluating reactor components and experiments.

Experimental Work:

Compact toughness specimens (2 mm thick, 10 mm square) were machined from a 20% cold-worked and stress-relieved Zircaloy-2 pressure tube that was originally manufactured in the 1960s (Sn 1.47 wt.%, Fe 0.12 wt.%, Cr 0.11 wt.%, Ni 0.06 wt.%, O 1010 wt.ppm, H 12 wt.ppm, balance Zr); the notch was not examined in this experiment. The microstructure comprised flat α-grains with thickness of about 1 μm, elongated to about 10 μm in the axial and transverse directions. The zirconium crystals had a preferred orientation with respect to the principal directions of the tube, axial (A), radial (R) and transverse (T) directions, with Kearns' factors [41] for (0001) of $f_A = 0.046$, $f_R = 0.376$, and $f_T = 0.578$. Tensile properties of the Zircaloy-2 material were obtained in the transverse direction using ASTM Standard methods [42, 43]. The yield strength was found to obey the empirical relation: $959-1.95T+2.77x10^{-3}T^2$ [MPa] for temperatures, T(^{o}C), between 100 ^{o}C and 350 ^{o}C.

Hydrogen was added gaseously to two Zircaloy-2 specimens to concentrations of 0.6 at.% and 1 at.%. A third reference specimen was fabricated, but without added hydrogen; its as-received hydrogen concentration was 0.1 at.%. At the conclusion of the X-ray experiments described below, each specimen was completely sectioned into six separate samples. Differential Scanning Calorimetry (DSC) (TA Instruments) was used to measure the heat flow during heating and cooling at 10 ^{o}C/min about the expected solvus values for each sample. Typical DSC curves for the specimen with 1 at.% hydrogen in Zircaloy-2 are shown in Figure 3. The heat flow shows the endothermic energy, interpreted as that required to dissolve hydrides on heating, passed through a minimum at 315 °C ± 7 °C, and the onset of exothermic energy released, interpreted as that emitted when hydrides precipitate on cooling, occurred at 278 °C ± 4 °C. Similar measurements for the 0.6 at.% specimen showed the minimum heat flow on heating occurred at

282.4 °C ± 2 °C, and the onset temperature on cooling was 255.3 °C ± 2 °C; the corresponding temperatures for the 0.1 at.% specimen were 172 °C ± 9 °C and 141 °C ± 3 °C. The temperature differences for dissolution and precipitation for these specimens range from 27 °C to 37 °C. Reported DSC temperatures are averages and standard deviations determined from three runs for each of the six sectioned samples of each specimen. Hydrogen concentrations were measured with Hot Vacuum Extraction Mass Spectroscopy (HVEMS) [44]. The determined average atomic percent concentrations and standard deviations for hydrogen were 1.02±0.04, 0.57±0.04, and 0.11±0.03, corresponding to ppm by weight values 113±4, 63±4, and 12±3, respectively.

X-ray diffraction experiments were performed with the Advanced Photon Source Synchrotron at Argonne National Laboratory on beamline 1-ID. The beam was calibrated with a ceria standard; the wavelength was 14.42 pm; it was rectangular (200 μm x 50 μm) and incident normal to the square surface of the specimen in the radial direction of the original tube. The transverse direction of the original tube was vertical and the specimen was held stationary with a 10 N load used to secure it in the load frame. The beam passed through the specimen sampling about 200 000 α-grains. The test temperatures were obtained with a furnace that surrounded the specimens and grips, and the temperature was measured and controlled with a thermocouple spot welded to the side of the specimen [45]. An illustration of the experimental arrangement is shown in Figure 4.

Diffraction rings were collected on an amorphous silicon detector located 2 m behind the specimen to magnify the region where γ- and δ-hydride signals are expected with d-spacings between 0.26 nm and 0.28 nm corresponding to {111}. Figure 5 shows that the intensities of the zirconium diffraction rings varied with angle around the ring because of the underlying crystallographic texture of the zirconium lattice. The majority of basal-plane normals in the specimens were aligned in the vertical direction, which is the transverse direction in the original tube, and the prism plane normals were aligned horizontally. The major intensities of diffraction from the zirconium (0002) were at the top (0°) and bottom (180°) of the diffraction rings.

Figure 6 shows room temperature zirconium metal diffraction peaks obtained by integrating the intensity around the diffraction rings for the 0.1 at % (12 ppm) hydrogen specimen. Diffraction lines associated with the basal (0002) plane and prism $\{10\bar{1}0\}$ plane are labeled in the spectrum; for the diffraction pattern obtained at each location in the specimen, the intensity is normalized to the strongest line, which is the pyramidal $\{10\bar{1}1\}$. Zirconium metal has a hexagonal-close-packed crystal structure with lattice parameters measured in this work at 25 °C: a_0 = 0.323 nm and c_0 = 0.515 nm, as expected [46].

Hydrogen in solution expands the zirconium proportional to the concentration: for example, at 450 °C, 1 at.% hydrogen increased the a-lattice spacing by 1.13 x 10^{-4} nm and the c-lattice spacing by 2.95 x 10^{-4} nm, providing an anisotropy factor of 2.61 [47]. Thus, changes in zirconium lattice spacings are a measure of both changes in the concentration of hydrogen in solution and thermal expansion.

Hydrogen can leave solution to form hydride phases in the zirconium lattice, and additional peaks appear in the diffraction spectrum. In this work, hydride peaks were seen because of the face-centered-cubic δ-phase, with a lattice parameter at room temperature of 0.478 nm [48, 49],

and the γ-phase, which has a face-centred-tetragonal (c/a>1) structure, and reported lattice parameters at room temperature a = 0.460 nm and c = 0.497 nm [48, 49] and a = 0.459 nm and c = 0.495 nm [50]. Consequently, at room temperature hydrides expand the zirconium lattice locally by 12% to 17% [51, 52]. Figure 7 shows the region of the diffraction spectrum where peaks associated with diffraction from {111} planes of γ- and δ-hydrides can be found for the three hydrogen concentrations of this study at room temperature. The d-spacing for the {111} peaks calculated from the lattice parameters [53] are 0.276 nm for δ-hydrides, and 0.272 nm and 0.271 nm, respectively, for γ- hydrides. The d-spacings in Figure 7 are lower than these calculated values because in this study the X-rays traverse the specimen so that the hydrides diffracting the beam are in compression in the metal interior. X-ray diffraction patterns seen in reflection have higher d-spacings from hydrides closer to the metal surface where any compressive stress will be relieved. Similar low d-spacings of the {111} δ-hydride peak in Zircaloy-4 have been reported in another synchrotron transmission X-ray diffraction study [45].

The amounts of γ- and δ-hydride were determined by integrating the intensity of the diffraction peaks from {111} planes of each hydride phase around the circumference of the diffraction rings, and in two angular ranges around the diffraction rings: 0^o to 20^o and 55^o to 75^o counterclockwise from the top. The amounts of hydrides were assumed to be proportional to the areas of the diffraction peaks.

Diffraction spectra were obtained under isothermal conditions at temperature intervals between room temperature and 330 °C. The specimens were heated and cooled at 10 ^{o}C/min between temperature intervals of 10 °C or 5 °C between 200 °C and 330 °C, followed by an isothermal hold of 3 minutes before spectra were collected every 0.5 s for 18 s. The isothermal hold facilitates both thermal equilibrium and equilibrium between hydrogen in solution and hydrides, but equilibrium is not required to interpret these isothermal diffraction spectra with dynamic DSC heat flow measurements. The data obtained during cooling were gathered after the data obtained during heating, which included annealing at 550 °C for an hour that ensured all of the hydrides were dissolved.

Theory:

The Einstein relation for Brownian motion [7] is used to describe diffusion when velocities of particles are limited to terminal values, such as ions moving in liquids under applied electric potential gradients (*i.e.*, Nernst-Einstein equation), particles moving in viscous liquids under gravitational potential gradients (*i.e.*, Stokes-Einstein equation) and the drift current in semiconductors. Solute atoms moving in solid solutions reach terminal velocities, ν, that are proportional to forces derived from negative gradients in chemical potential: $v = -\Gamma \nabla \mu$. The proportionality constant is the mobility, Γ. The chemical potential is written using the definition of relative activity of the solute, a, *via* $\mu = \mu^o + RT \ln a$, where T is temperature in K, R is the Ideal Gas Constant, 8.314 J/mol.K, and μ^o is a reference state for the chemical potential [54]. The activity is approximated by concentration, C, in the limit of ideal dilute solute, which will be assumed in accord with the solute (hydrogen) in the solid solvent (zirconium) being less than 1 at.% in this study. The chemical potential includes an additional term to account for the work done to expand the solvent (e.g. by the solute), so that regions of tension lower the chemical potential; this work is the product of the hydrostatic pressure, σ, and the partial molar volume, V, of the solute. The flux of solute, J, is the product of the velocity and the concentration. The flux

reduces to the empirical equation of Fick [55] when there are no temperature or stress gradients (*i.e.*, $\mathrm{J} = -D\nabla C$, which defines the diffusion constant, D); the equivalence of the flux and Fick's equation leads to the Einstein relation between the mobility and the diffusivity: $\Gamma = D/RT$. Thus, Fick's Law is derived from the chemical potential. Inserting the gradient of the chemical potential into the equation for the velocity, multiplying by the concentration to give the flux, and substituting the Einstein relation for the mobility, yields the Einstein flux in a hydrostatic stress gradient at constant temperature in terms of the diffusivity [8]:

$$\mathrm{J} = -D\left(\nabla C + \frac{CV}{RT}\nabla\sigma\right). \qquad (3)$$

The flux of solute atoms, J, contains a diffusion current, which depends on concentration gradients as in Fick's Law, and a drift current, which depends on stress gradients. Equilibrium is defined when the chemical potential of hydrogen is the same in all phases, which is equivalent to J = 0. Equilibrium is temperature dependent because the drift current and diffusivity both vary with temperature.

The simple no-flux solution to Equation 3 is for no gradients in concentration and stress. This solution can be used to define the solvus, which is a unique temperature and concentration of hydrogen in solid solution in dynamic equilibrium with hydrogen at a hydride surface in the volume adjacent to the surface in the limit where any stress gradients are zero. Similar approaches are used to truncate the stresses at the tip of a sharp crack, which defines an event horizon to avoid a singularity [56, 57]. The hydrides that form will be under compression, and the adjacent metal lattice will be under tension. Between these regions of compression and tension is the neutral stress region, where the stress gradient is zero, and, by Equation 3, where there will be no concentration gradient at equilibrium. These two conditions define the solvus in terms of the concentration of hydrogen in solution in the volume adjacent to the hydride surface in the limit where any stress gradients are zero.

Consider cooling gradient-free zirconium alloy containing hydrogen completely in solution. Just before precipitation there are no concentration gradients, and there are no stress gradients associated with matrix hydrides, because there are none. The onset of precipitation will be used to approximate the temperature for the no-gradients condition that defines the solvus temperature associated with only one concentration. This concentration is the solvus, or the terminal solid solubility, C_{TSS}. This value was used to predict the maximum in delayed hydride cracking growth rates in zirconium alloys [8] and will be used to explain the observations of this work.

Additional no-flux solutions to Equation 3 occur when the two gradient terms are equal and opposite. Thermal fluctuations can lead to transient local concentration gradients in embryonic condensations of hydrogen clouds, and accompanying stress gradients because of the hydrostatic stress from the hydrogen atoms, but these structures will be dissipated by thermal agitation until hydrides form. When hydrides are present, stress gradients will form as the metal is expanded because of the larger volume of metal hydrides compared with the metal. Stable stress gradients also form in response to internal defects and external loads. When stable hydrides are present, there will be regions where local concentrations are stabilized at the solvus concentration; concentration gradients within the hydrogen clouds will terminate with the solubility limit. Equilibrium concentrations of hydrogen in solution in the presence of hydrides and stress

gradients are determined by setting the flux of hydrogen in Equation 3 to zero and integrating with one concentration limit equal to C_{TSS}. There are two possibilities:

$$\int_{C_-}^{C_{TSS}} \left(\frac{\nabla C}{C}\right) = -\int \frac{V\nabla\sigma}{RT}; \quad \int_{C_{TSS}}^{C_+} \left(\frac{\nabla C}{C}\right) = -\int \frac{V\nabla\sigma}{RT}. \tag{4}$$

At these limits, the difference in hydrostatic stress is negatively proportional to the yield stress, σ_y, for tensile stress gradients. The proportionality constant is the elastic stress concentration factor, K, which is expected to vary between 1 and 2.4, the latter being the value in the plain-strain limit, appropriate for needle-like γ-hydrides, in a lattice that deforms in a perfectly plastic manner [56-59]. The two solutions for tension depend on the ordering of the integration limits:

$$C_-(T) = C_{\mathrm{TSS}}(T)\exp\left(\frac{-KV\sigma_y}{RT}\right); \tag{5}$$

$$C_+(T) = C_{\mathrm{TSS}}(T)\exp\left(\frac{+KV\sigma_y}{RT}\right). \tag{6}$$

Different values of K may be possible for different internal defects, for example, dislocations, that give rise to local gradients in hydrostatic stress seen by the solute. For example, Equations 5 and 6 are plotted in Figure 8 for $K = 2$.

Equation 5 corresponds to when the hydrogen concentration in solution equals C_{TSS} at the stress riser and C_- in the neighbouring matrix, which first happens at T_+ when cooling from a temperature where all the hydrogen is in solution (Figure 8). The hydrogen flux also equals zero when the hydrogen concentration in solution equals C_{TSS} at the stress riser and C_+ in the neighbouring matrix. At temperature T_- shown in Figure 8, the concentration of hydrogen in solution in the matrix neighbouring the stress riser equals the total hydrogen concentration. The hydrogen in solution in the matrix neighbouring the stress riser can form equilibria with subsequent neighbouring regions when the concentrations satisfy J = 0. For concentrations and temperatures bounded by the expressions for C_+ and C_-, the flux of hydrogen, J, is negative and hydrogen moves from the surrounding matrix to the hydride, otherwise J is positive and the hydrides lose hydrogen to the solution. Thus, hydrides are predicted to be stabilized against dissolution above the solvus temperature until T_+, and destabilized and dissolve below T_-. The drift current directed towards tensile stresses emanating from lattice imperfections such as dislocations or from hydrides already formed, can inhibit dissolution, which can lead to hydride precipitation above the phase boundary, and hydride dissolution below the phase boundary. These solutions given by Equations 5 and 6 do not yield a solvus, by definition, because the concentration of hydrogen in solution is not unique due to the concentration gradient. Concentration varies with location, notably one concentration at the stress riser and a second concentration far-field in the matrix.

Equation 5 has been proposed before to explain how delayed hydride cracking can occur above the solvus on cooling from temperatures where all of the hydrogen is in solution: hydrides are stabilized at the crack tip by the drift current once T_+ is reached (see Figure 6 in [8] where T_+ is called T_5). Equation 6 is proposed in this work to represent the concentration of a hydrogen

cloud formed at a stress concentration or a Cottrell atmosphere of hydrogen in solution at a dislocation [60]. The concentration in the hydrogen cloud or Cottrell atmosphere can be higher than the solvus concentration when it is stabilized by the drift current, and can be destabilized for concentrations and temperatures above the line for C_+, Equation 6.

Results:

The areas of hydride diffraction peaks were found to increase as hydrides precipitated and decrease as hydrides dissolved, and spacings of the zirconium lattice were found to expand and contract in accord with hydrogen moving in and out of solution. Figure 9 shows the areas of hydride peak intensities integrated around the circumference of the diffraction ring for the specimen with 1 at.% hydrogen, (113±4) ppm. On cooling from a temperature where all of the hydrogen is in solution (370 ^{o}C), γ-hydride diffraction peaks were observed at 330 ^{o}C. The area of these γ-hydride diffraction peaks decreased to a minimum value at ≈315 ^{o}C, coincident with the minimum heat-flow temperature on heating shown in Figure 3, and T_+. With further cooling, the areas of the γ-hydride diffraction peaks increased as the temperature was lowered past the onset of precipitation temperature (*i.e.*, the solvus or TSS: 280 ^{o}C, Figure 3), and reached a maximum value at ≈245 ^{o}C, which is coincident with T_-. (The calculation of T_+ and T_- is described in the Discussion.) δ-hydrides were not observed during cooling until 230 ^{o}C. On heating, γ-hydride peak intensities integrated around the ring were not discernible from the variability in the background. The areas of δ-hydride peak intensities integrated around the ring were seen to rise with heating to a maximum value at 230 ^{o}C, and then fall with further heating. For temperatures above 280 ^{o}C, the δ-hydride peaks were not distinguishable from the variability in the background.

The large intensities of adjacent zirconium diffraction peaks makes it difficult to see small hydride peaks. This large confounding background can be reduced with a judicious choice of viewing angles for the hydrides between the regions where the texture makes the zirconium lines intense. The hydrides can be seen relatively free of zirconium interference between 0^{o} to 20^{o} and 55^{o} to 75^{o} from the top of the diffraction rings.

Figure 10 shows stacked plots of integrated intensity from 0^{o} to 20^{o} and 55^{o} to 75^{o}, from the top of the diffraction rings, obtained with the specimen containing 1 at.% hydrogen for a series of isothermal measurements made at progressively higher temperature in the region where γ- and δ-hydride peaks are found. The temperatures of the stacked spectra range from 220 °C to 310 °C (top to bottom) in steps of +10 °C, with each spectrum offset vertically from the low temperature spectrum. Both the γ- and δ-hydride peaks persisted to temperatures above the onset precipitation temperature, and disappeared when the temperature reached the minimum heat-flow temperature determined during heating with DSC.

Figure 11 shows stacked plots of diffraction spectra obtained with the specimen containing 1 at.% H for a series of isothermal measurements made at progressively lower temperature. The temperatures of the stacked spectra range from 330 °C to 230 °C (top to bottom) in steps of -5 °C, with each spectrum offset vertically from the low temperature spectrum. Prior to these measurements the specimen was heated to 550 °C for an hour to ensure all of the hydrides were dissolved. Figure 11 shows the integrated intensity from 0^{o} to 20^{o} and 55^{o} to 75^{o} from the top of the diffraction rings. Common to both views in these figures, there is no indication of δ-hydride

until the lowest temperature of 230 °C is reached. In both angular views, the γ-hydride peak seen at the starting temperature, 330 °C, decreases as the temperature is lowered to ≈315 °C, then rises to a maximum value at an intermediate temperature that depends on the view, before falling again as the temperature is lowered to 230 °C.

Figure 12 shows stacked plots of diffraction spectra obtained with the 0.6 at.% H specimen for a series of isothermal measurements made at progressively lower temperature. The temperatures of the stacked spectra range from 300 °C to 200 °C (top to bottom) in steps of -5 °C, with each spectrum offset vertically from the low temperature spectrum. Prior to these measurements the specimen was heated to 550 °C for an hour to ensure all of the hydrides were dissolved. Figure 12 shows the integrated intensity from 0^o to 20^o and 55^o to 75^o from the top of the diffraction rings. There is no indication of δ-hydride on cooling until 205 °C. The γ-hydride peak in the 0^o to 20^o view is first seen on cooling at 280 °C; the peak grows reaching a maximum value on further cooling, and then disappears by ≈235 °C. Compared with the specimen containing 1 at.% H, for the 0.6 at.% H specimen there is no indication of γ-hydride in the 55^o to 75^o view, outside of the limits inferred for the background, and, in the 0^o to 20^o view, signals associated with δ-hydrides at low temperatures are difficult to distinguish from the background.

The diffraction lines for 0.6 at.% H in Zircaloy-2 shown in Figure 12 confirm features seen in Figure 11 for 1 at.% H: on cooling, γ-hydrides are seen to form above the DSC onset precipitation temperature in the 0^o to 20^o view; the diffraction lines associated with these γ-hydrides grow reaching maximum values below the onset precipitation temperature, and then decline, and disappear in the 0.6 at.% H specimen, before δ-hydrides are seen in both views, which happens 50 °C below the onset precipitation temperature.

Figure 13 shows how the areas under the diffraction peaks from {111} planes of the γ-hydrides and δ-hydrides (subsequently called area) vary with temperature during cool-down, and heat-up for the specimen with 1 at.% H. These plots show qualitatively how the amounts of various hydrides change as they precipitate and dissolve at various temperatures. The areas of the γ-hydride lines on cooling have been normalized to their maximum values on cooling, and the areas of δ-hydride lines on heating are normalized to their maximum values on heating.

The d-spacings for the $\{10\bar{1}0\}$ and (0002) alpha zirconium lines, with thermal expansion subtracted, determined from the specimen containing 0.1 at.% H, are depicted in Figure 14. These plots corroborate hydrogen moving into and out of solution; d-spacings increase or decrease when hydrogen moves into or out of solution. In both plots, the values were raised and lowered so that the high temperature results overlapped. The values after cooling were lower than those for heating presumably because of the stress relief within the specimen after the 550 °C heat-treatment. Similar results were seen for the zirconium lines of the specimen containing 0.6 at.%. The cooling results for the specimen containing 1 at.% H are discussed first.

Figure 13a shows that on cooling from temperatures where all of the hydrogen is in solution, γ-hydride diffraction lines are observed to form above the temperature of minimum endothermic heat-flow seen on heating (315 °C; Figure 3), and at both diffraction-ring viewing ranges between 55° and 75° and between 0^o and 20^o from the top of the diffraction ring. These γ-hydrides are clearly visible in the diffraction data, appear to be transient and they do not appear to contribute to the heat flow measured with DSC during cooling (Figure 3). The hydrides

diffracting between 0^o and 20^o grow below 315 °C and, because they continue not to contribute to the heat flow, at least until 280 °C, they are labeled with the superscript '^{a}' to connote that these hydrides are apparently athermal.

On cooling a further 35 °C, at diffraction-ring angles between 55^o and 75^o, γ-hydride diffraction lines again become visible at the temperature of the first indication, or onset (TSS), of exothermic heat flow observed in the DSC experiment (280 °C, Figure 3) and continue to grow on cooling; they are called 'thermal' γ-hydrides, and labelled γ^t, even though these hydrides were apparently athermal for temperatures above 315 °C for the isothermal X-ray diffraction measurements shown in Figure 13a.

The different diffraction-ring angles where γ^a and γ^t are observed suggests these hydrides precipitate on different planes in the textured zirconium matrix. Although the amount of γ^a-hydride might appear to be large in Figure 13a, recall that these areas have been normalized, and the intensities in the angular collection ranges are not necessarily similar. The amount of hydrogen leaving solution inferred from the changes in zirconium lattice spacings integrated around the ring shown in Figure 14 provides a better indication of the relative amounts of γ^a and γ^t for the measurement temperatures. The amount of γ^a-hydride should provide an exothermic signal but it is too small to resolve with the current DSC instrument.

On further cooling, γ^a and γ^t precipitation reaches maximum amounts at 260 ^{o}C and at 245 ^{o}C, respectively. On still further cooling, the areas for these γ-hydrides decrease. These hydrides are dissolving and hydrogen is going into solution as indicated by the increase in zirconium lattice parameter in Figure 14 starting at 250 ^{o}C. The γ-hydrides dissolve at temperatures above where δ-hydrides appear suddenly at 230 ^{o}C in both viewing angles (Figure 13a). The sudden appearance of δ-hydrides is shown in Figure 15 by the time-dependent growth of the δ″-hydride peak between 55^o and 75^o; the γ^t-phase peak decreases over the same time. Unlike the decline of the γ^t-phase, the increase in δ″-phase did not reach equilibrium in the 18 s observation time, which occurred after cooling from 235 ^{o}C to 230 ^{o}C, at 10 ^{o}C/min, and then waiting for 3 min (Figure 16). The α-phase lattice parameter declined when the specimen was cooled from 235 ^{o}C to 230 ^{o}C (Figure 14), but it remained constant over the 18 s observation time of Figures 15 and 16, which suggests prior hydrogen accumulation in the regions where δ-hydride precipitated. No extra heat was detected by DSC at the temperature where the δ-phase started to precipitate between 235 °C and 230 °C, Figure 3.

Figure 13b shows that on heating from 220 °C, the γ^t-hydride areas increase as the temperature is increased (thus hydrides are forming), reaching a maximum around 265 ^{o}C, and then dropping to a low value at ≈280 ^{o}C. The δ′-hydride areas increase until 240 ^{o}C (these hydrides are also forming during heating), but then dissolve and are gone by ≈ 315 ^{o}C. The δ″-hydride areas decrease monotonically with heating. The γ^a-hydride areas are difficult to quantify in Figure 10 (bottom plot): although the peak intensities are changing, with the peak widths increasing above ≈280 ^{o}C, the peak areas seem almost constant over the temperature range. Figure 14 shows that the d-spacings of the zirconium lines increase monotonically with increase in temperature: there is no hiatus.

Precipitates in metals that dissolve on cooling and form on heating: an example with hydrogen in alpha-zirconium

Discussion

The $T_{\pm}$ temperature limits shown in Figures 9, 13 and 14 were calculated with the temperature dependence of the solvus (TSSP in [61]), the partial molar volume of hydrogen [45], and the yield strength determined in this work. For the current solvus (TSS) temperature, which is equal to the DSC onset temperature for precipitation on cooling (280 ^{o}C, Figure 3), the calculated plain-strain perfectly-plastic upper limit for T_{+} is 320 ^{o}C, which agrees well with the temperature where hydrides disappear on heating, and γ^{a}-hydrides appear on cooling, ≈315 ^{o}C (Figure 13).

The plain-strain perfectly-plastic lower limit for T_{-} is calculated to be 237 ^{o}C. Experimentally the temperature where the γ^{t}-hydrides dissolve (Figure 13a) and hydrogen goes into solution (Figure 14) is between 245 °C and 250 °C. If instead the K factor multiplying the yield stress is reduced from the plain-strain perfectly-plastic value of 2.4 to 2.0, then T_{+} becomes 314 °C and T_{-} becomes 245 °C, which agree with the observed experimental temperatures; these temperatures are indicated as vertical lines in Figures 9, 13 and 14. Equations 5 and 6 are plotted in idealized form in Figure 8 along with the $T_{\pm}$ temperature limits calculated with K = 2. Crack-tip stresses in the plain strain limit have been characterized with similar values of multiples of the yield stress [63] suggesting that the stress fields around hydrides are similar to those found at crack tips in plain strain. Figure 8 indicates the regions where the flux of hydrogen is initially positive (leading to hydride dissolution) or negative (leading to hydride formation) during heating and cooling when hydrides are present or can form given time – these positive and negative fluxes are not general, they correspond to specific examples described below. An example where the initial flux designations in Figure 8 would not apply is for temperatures well above T_{+}, where the initial flux will be negative and hydrogen will flow to regions of tension, but no stable hydrides would form. Eventually, the flux would go to zero when equilibrium is achieved. Hydrogen concentration gradients without precipitates have been observed in zirconium bars subjected to bending stresses [62].

Hydride precipitation and dissolution during cooling and heating is controlled by the concentrations C_{+}, C_{TSS}, and C_{-}. At a constant temperature, equilibrium is when the concentration of hydrogen in solution at the hydride surface is C_{TSS} and surrounding layers have concentrations of C_{+}, C_{TSS}, or C_{-} (i.e., J = 0). When the temperature first changes during heating or cooling, the local concentrations do not change instantly, which on Figure 8 would be represented by moving concentrations along horizontal lines, so the concentrations C_{+} and C_{-} that were present at the equilibrium temperature will move either into regions where J > 0 or J < 0. For cooling, the initial C_{-} moves into a J < 0 region and is stabilized. The initial C_{+} concentration moves into a J > 0 region and would dissolve except for the stress has been relieved by the influx of hydrogen forming a hydrogen cloud. This initial state is stable on cooling until the initial C_{TSS} intersects with the C_{+} line, demonstrated with the top horizontal line in Figure 8; this intersection happens at the TSS (solvus) temperature. The initially formed hydrides dissolve at this point, and new hydrides appear in unstressed regions of the matrix. These events are ultimately controlled by the C_{+} line.

For heating from an initial equilibrium state, the reverse happens, and the events are ultimately controlled by the C_{-} line. When heating from an initial equilibrium, C_{-} moves into a J > 0 region and dissolution occurs. Heating moves C_{+} into a J < 0 region, and the C_{+} concentration grows

because the stress gradient diminishes, perhaps reaching sufficient values for condensation of hydrogen. This initial state is stable on heating until the initial C_{TSS} intersects with the C_- line.

On cooling: hydrides can form and dissolve

It follows that the first hydrides to form on cooling, the athermal γ^a-hydrides, must be precipitating in regions where there are prior stress gradients and concentration gradients, because they form above the solvus temperature. We propose that hydrides observed below 315 °C between 0^o and 20^o around the diffraction ring are associated with dislocations. Hydrides are suggested to form when hydrogen trapped by tensile stresses at crystal imperfections (e.g. dislocations) attain concentrations sufficient to precipitate hydrides. Metals contain imperfections in the lattice that produce local tensile stress gradients, and there are many sites of residual stresses, for example from intergranular differential thermal expansion, that will encourage hydrogen to flow and form precipitates in the same way as to a crack tip under an applied tensile stress [8]. The internal stresses would activate the drift current and promote precipitation above the solvus temperature, hence γ^a-hydrides are predicted.

Figure 17 shows hydrides decorating dislocations is possible. The precipitates form well above the onset temperature in Figure 3 and appear to be athermal. If kinetic energy of the hydrogen is lost when associating with the imperfection, then the chemical energy released might appear to be small. The aggregation of hydrogen atoms in the tensile region relieves hydrostatic stresses when the elastic dilation caused by the dislocation has been replaced by the dilation associated with the different atomic volumes of solute and solvent: Cottrell atmosphere [60].

When hydrides form, the concentration of hydrogen in solution at the hydride edge will be at the solubility limit, $C_{TSS,}$ for the formation temperature. Hydride formation introduces additional stress and further hydrogen movement to form an additional hydrogen cloud with concentration C_+ that surrounds the region at C_{TSS}. As the temperature is lowered, hydride growth is stunted: initially hydrogen moves towards the hydride because $J < 0$, until the additional stress associated with the hydride is relieved, at which point $J = 0$ and there is no hydrogen flux to grow the hydride. These hydrides once formed do not grow when cooled, until a temperature is reached where $J > 0$ at the periphery of the second hydrogen cloud so that the hydrogen in solution trapped at the hydride edge can diffuse away and the hydride will dissolve. A consequence of hydrides being unable to grow when cooled is that they form into arrays of platelets, which are discussed later.

The γ^a-hydrides that form above the solvus temperature are predicted to dissolve in the order they were formed as the temperature is lowered below the solvus temperature, and be gone by T_-. The result is that a maximum amount of γ^a-hydrides should be seen between the solvus temperature and T_-. The sequence of events is depicted in Figure 8. γ^a-hydrides that form above the solvus temperature will decline following C_+ below the solvus (seen as the intersection of the horizontal grey lines with C_+). The γ^a-hydrides that form below the solvus temperature will increase with cooling as do the vertical grey lines seen in Figure 8 below the solvus. The net difference predicts a maximum hydride diffraction peak area at 260 ^{o}C, which agrees with the observed maximum temperature.

Precipitates in metals that dissolve on cooling and form on heating: an example with hydrogen in alpha-zirconium

On further cooling below T_-, and to the left of the (C_+, J=0) line in Figure 8, the flux becomes positive and hydrides dissolve. In Figure 13a, around 250 °C, we see the areas for γ'-hydrides decreasing, and in Figure 14 the zirconium lattice-spacing increasing, which confirms the hydrides are dissolving during cooling and hydrogen is going into solution. The γ'-hydrides continue to dissolve, and a peak is seen in zirconium lattice spacing at a temperature below T_-. Then formation of δ-hydrides intervenes. The γ-hydrides cannot simply transform to δ-hydrides; the large stoichiometry difference has to be overcome and there is not enough hydrogen in the (ZrH) γ-hydrides to form ($ZrH_{1.5\text{-}1.67}$) δ-hydrides. The γ-hydrides would have to collapse to a smaller volume while rearranging hydrogen bonding if the δ-hydrides were formed strictly from solid-state conversion of γ-hydrides. In addition, if γ-hydrides were transforming into δ-hydrides by solid-state conversion, the rates of change of the areas of hydride diffraction peaks would sum to zero. Figure 16 shows that during the 18 s observation period after the cooldown to 230 °C and hold, the γ-hydride signal remains almost constant after ≈10 s while the area of the δ-hydride peak continues to grow, hence, solid-state conversion is not supported by the time dependence of the hydride diffraction signals.

Instead, the γ'-hydrides dissolve putting hydrogen into solution, including into the surrounding hydrogen cloud and into the metal matrix. This hydrogen is available when the higher stoichiometric δ-hydrides form as the temperature reaches 230 °C for the specimen containing 1 at.% H. The ratios of C_+ to C_{TSS} calculated from Equation 6 vary from 1.6 to 1.7 as the temperature is reduced from 280 °C to 230 °C provide the range of stoichiometry for the δ-hydride. The concentration of hydrogen in solution drops suddenly as the δ-hydride forms, as demonstrated by the last of the cooling points in Figure 14 showing the decrease in lattice parameter for the zirconium lines between 235 °C to 230 °C, and the sequential growth of the δ-hydride peaks shown in Figure 15 and Figure 16. Consistent with hydrogen condensing from the local hydrogen cloud, there was no further movement of the zirconium diffraction lines during the sequential growth showing that the required amount of hydrogen in solution had already moved to the regions where the δ-hydride formed in the time between the start of cooling from 235 °C and the start of the measurement at 230 °C. The amounts of γ-hydride and δ-hydride may vary in this concerted way with further cooling.

In the specimen with 0.6 at.% H, on cooling, δ-hydrides were observed to form suddenly well below the solvus temperature in a similar manner as observed for the specimen with 1 at.% H. Figure 12 shows the process seen for 1 at.% H is repeated in the specimen with 0.6 at.% H, except the formation of δ-hydrides occurs at 205 °C. The lower temperature (205 °C versus 230 °C) is in accord with the lower solvus temperature (255.3 °C ± 2 °C versus 278 °C ± 4 °C) because of the lower concentration (0.6 at.% H versus 1 at.% H) in the specimen. For both specimens, γ-hydrides formed above the solvus temperature on cooling, and then on further cooling δ-hydrides formed 50 °C below the solvus temperature after γ'-hydrides dissolved. For both specimens, hydrogen moving in and out of solution was corroborated by the change in d-spacings observed for the zirconium lines.

Figure 7 shows that the room-temperature proportions of γ-hydride and δ-hydride in the Zircaloy-2 specimens of this study changed in a similar manner as reported for low hydrogen concentrations in pure zirconium [9, 10, 11] and in Zircaloy-4 [12] and in Zr-2.5Nb [16-19] (See the background in the Introduction). At low concentrations, 0.1 at.% H, only γ'-hydrides were

observed. For 0.6 at.% H and 1 at.% H, both γ-hydrides and δ-hydrides were observed, with a greater proportion of δ-hydrides for the larger total hydrogen concentration. The areas of the γ-hydride peaks are similar for the three concentrations. If the events leading to the precipitation of δ-hydrides seen in Figures 11, 12, 13 and 14 can serve as a template, then hydride formation starts with γ-hydride precipitation, and follows with dissolution of some γ-hydrides at temperatures below the solubility limit, and then δ-hydrides precipitate below T_-. The dissolution of γ-hydrides will take longer for lower total concentrations of hydrogen because the diffusion rates are lower because the temperatures are lower. The preponderance of γ-hydrides at low temperatures for low total hydrogen concentrations could result from insufficient time for the γ-hydrides to dissolve so that δ-hydrides can precipitate, for example, during an experiment. For higher total hydrogen concentrations, for which temperatures are also higher, the diffusion times will be shorter. The implication is that γ-hydrides are expected to dominate for low concentrations, and δ-hydrides dominate for high concentrations, in specimens with similar cooling when compared at room temperature.

The decreasing and then increasing of the lattice spacings in Figure 14 during cooling, and then the drop once δ-hydrides precipitate shows that the concentration of hydrogen in solution below onset precipitation temperatures cannot be captured with a simple universal function (e.g. exponential). For instance, specimens with low total hydrogen concentrations need to be cooled to low temperatures to instigate precipitation, but diffusion is slow at low temperature, and precipitation of δ-hydrides might be indeterminately delayed. Hence, the concentration of hydrogen in solution could be higher than expected from extrapolation of TSS precipitation onset values determined with DSC at higher temperatures. A disproportionately small, or absent, δ-hydride peak could indicate hydrogen frozen in solution. The implication is that models of phenomena that depend on the concentration of hydrogen in solution, such as delayed hydride cracking [8], could under-predict rates at low temperatures and low concentrations. There are indications that TSSP features change with temperature history [64], seemingly suggesting complicated precipitation, whereas the current results show both precipitation and dissolution behaviour, Figures 13 and 14. In contrast, experimentally determined TSSD concentrations vary smoothly with temperature on heating, like the lattice spacings for the zirconium lines in Figure 14.

Figure 13 show hydrides on cooling above T_+, for reasons that are not yet clear. The zirconium lattice contracts when cooled squeezing hydrogen into regions of relative tension where the concentration could locally exceed C_-, even though the average concentration would not. Thus, a second 'rainbow' line (C_{--}) could be defined below C_-. Similarly, hydrides above T_+ also suggests additional no-flux conditions with different values for K. Regions of compression will likewise lead to no-flux equations like those for tension (Equation 4). Compressive yield strengths can be higher than tensile yield strengths, and could be different depending on direction for a textured matrix.

On heating: hydrides can dissolve and precipitate

Figure 13b shows the areas of δ″-hydride diffraction peaks decrease as the temperature is raised; hydrides in this view were previously labelled thermal. The areas of δ′-hydride diffraction peaks increased with heating from 220 °C, and reached a maximum at ≈240 °C. Figure 8 suggests the maximum should occur at 250 °C, which is the temperature where a horizontal line from TSS at

220 °C intersects the C_- line. δ′-hydrides are seen in the view associated with imperfections such as dislocations. When heating first starts, the simultaneous increase of δ′-hydride and decrease of δ″-hydride combine to reduce the rate of increase of the amount of hydrogen entering solution, and a slow rise in d-spacings is seen initially in Figure 14 reminiscent of the horizontal line connecting Points C and D in Figure 2.

Figure 9 shows that on heating the total δ-hydride signal increases with temperature until 230 °C, which suggests that the increase for δ′-hydride is larger than the decrease for δ″-hydride over this initial heating range. Simultaneously, the hydrogen concentration in solution increases with heating, as shown by the rise in the d-spacings of the α-zirconium lines in Figure 14. Because the total amount of hydrogen in solution and as hydride is constant, the implication is that the γ-hydride phase must be suppressed when the total δ-hydride phase reaches a maximum value. When the total δ-hydride signal decreases above ≈240 °C, the suppression of the γ-hydride should cease, and the amount of γ-hydride increase, which can be seen in the rise of γ-hydride signal in Figure 10 above 250 °C. These concerted changes in γ-hydride and δ-hydride suggest that these phases are physically close.

The amount of γ^t-hydride decreased to a small value as the solvus was approached. γ^t-hydrides formed below the solvus temperature reached maximum values below the solvus, not above it, even though the flux is still negative above the solvus. Because the hydride lattice strain is relieved by hydrogen in solution at the periphery of a hydride, hydrides once formed do not dissolve when heated, until a temperature is reached where $J > 0$, (*i.e.*, when the C_- line is crossed) at which point the hydride will dissolve. The γ^t-hydrides that formed during cooling from 245 °C to 220 °C will reach C_- and begin to dissolve on heating at 250 °C, and should be completely dissolved by 280 °C. On heating, once the temperature passes 245 °C, γ^t-hydrides form, but most of these hydrides reach C_- and dissolve by 280 °C, with just a few lasting to 286 °C. Thus, the γ^t-hydride areas are predicted to increase at 245 °C, reach a maximum around 255 °C, and fall to low values at the solvus temperature, 280 °C, which is what is observed in Figure 13b.

Even though the areas of γ-hydride diffraction lines during heating become small for temperatures above the solvus, they do persist. The γ-phase is stable above the solvus on heating when $J < 0$. The process is self-stressing stabilizing where the sharp edges of hydrides put the local zirconium lattice into tension, which invokes the drift current, and hydrogen in solution is driven to the hydride, even though the solvus temperature has been exceeded. The drift current counteracts the dissolution current and stabilizes the precipitates to higher temperatures. For temperatures above T_+, J changes sign, and the hydrostatic stress imposed on the lattice by the sharp end of the hydrides is not enough to overcome the propensity of these hydrides to dissolve, and so they do.

The γ^a-hydrides do not follow the temperature dependence seen for γ^t-hydrides when heated. Figure 10 shows peak widths of γ^a-hydrides broaden for temperatures above T_{TSS}, while the areas of the peaks remain relatively constant, although the background in Figure 10 weakens definitive inferences. The γ^a-hydrides are possibly more stable at high temperatures because their stabilizing Cottrell atmospheres were also formed at high temperatures on cooling. Above the

772 solvus temperature, the γ^a-hydrides may experience a broadening range of stress from the
773 underlying dislocation as the hydrides become smaller.

774 The zirconium lattice spacings shown in Figure 14 vary smoothly with increase in temperature.
775 Eventually, on heating, the concentrations of hydrogen in solution associated with hydrides will
776 intersect with, and follow, the C_- boundary, which varies smoothly with temperature. For initial
777 heating, the increase with temperature of lattice parameters for the prism $\{10\bar{1}0\}$ diffraction lines
778 is less than for the basal (0002) line, which agrees with earlier work that suggests hydrogen in
779 solution more easily expands the crystal lattice along the c axis [47]. The relative changes in the
780 lattice parameters with temperature suggests that the anisotropy in the presence of hydrides is
781 temperature dependent. At high temperatures, when all of the hydrides have dissolved, the
782 contribution of hydrogen in solution to the ratio of lattice spacings, c/a, levels off to a constant
783 value [47].

784 ## Implications of the Phase Rule: a composite hydride with variable stoichiometry

785 For regions in the bulk metal where the chemical potential can be described in terms of two
786 intensive variables, concentration and temperature, there is one degree of freedom, as described
787 in the Introduction. The metal is ideal and defect-free. In these regions, there are no stress
788 gradients and the C_- and C_+ lines collapse about the central J=0 solution to Equation 3 shown in
789 Figure 8, which defines the solvus. The Phase Rule in these regions requires that for every
790 temperature there is a unique concentration of hydrogen in equilibrium with a unique hydride
791 phase, as in Equation 2. The solvus concentration is the total hydrogen concentration in the
792 metal in the limit as the temperature approaches the onset precipitation temperature on cooling –
793 the concentration of hydrogen in solution in the bulk does not change appreciably when
794 infinitesimally small amounts of hydride precipitate. At equilibrium, hydrogen in solution at the
795 hydride-metal interface is at the solvus concentration. In the volume where the solvus
796 concentration is defined adjacent to the hydride-metal interface, there are no net concentration
797 gradients, and, by Equation 3, there are no net stress gradients at equilibrium. In this gradient-
798 free volume, the Phase Rule dictates one degree of freedom.

799 Multiple hydride phases are not allowed at equilibrium if hydrogen also exists in solution. If
800 multiple hydride phases existed, then each hydride phase would have a similar region adjacent to
801 its hydride-metal interface where there would be no concentration gradients, and thus no stress
802 gradients. In each of these regions, an equilibrium concentration would exist that would be
803 different from the other equilibrium concentrations for the other hydride phases. But, these
804 different concentrations would cause hydrogen to flow to the hydride phase with the lowest
805 equilibrium hydride-metal interface concentration, by analogy with Ostwalt ripening where
806 precipitates with high local solute concentrations dissolve while precipitates with low local
807 solute concentrations grow [65]. If equilibrium concentrations can be defined in regions adjacent
808 to hydrides, then only one hydride phase can exist at equilibrium if hydrogen is in solution.

809 It follows that if there are two hydride phases, then at equilibrium there can be no hydrogen in
810 solution if there is a single degree of freedom. Simultaneous observation of two hydride phases
811 and hydrogen in solution suggests one hydride phase surrounded by another at equilibrium. The
812 sudden formation of δ-hydrides shown in Figure 15 and Figure 16 is therefore a non-equilibrium
813 process: δ-hydrides can never be in equilibrium with hydrogen in solution if γ-hydrides exist
814 simultaneously or are formed first. A single degree of freedom requires a composite hydride

forms with a single outer hydride phase, which can be either γ-hydride or δ-hydride. Which phase forms the outer layer between the hydride and hydrogen in solution may depend on rates of cooling and heating, and amounts of hydrogen.

When the δ-hydrides form, γ-hydride areas are observed to decrease, but γ-hydrides still exist in detectable amounts to the end of the observation period (Figure 15). If δ-hydrides form the outer hydride phase of the composite hydride, then the γ-hydrides must be completely surrounded and cut-off from hydrogen in solution to comply with the single degree of freedom. Figure 10 and Figure 13b show the signals from γ-hydrides change at the solvus temperature when heating: the areas of the γ^t-hydrides decrease appreciably, and the diffraction-line widths increase for the γ^a-hydrides. The γ-hydrides will only be sensitive to the solvus if they are in contact with hydrogen in solution, hence, δ-hydrides do not form the outer hydride phase of the composite hydride in this study.

When the δ-hydrides form, equilibrium can only be attained if the δ-hydrides are surrounded by a layer of γ-hydride, which would form when there is insufficient hydrogen available to form the higher stoichiometric δ-hydrides. Because γ-hydrides were the first to precipitate, probably because of stoichiometry and lower strain energy, this interpretation would require δ-hydrides to be surrounded by γ-hydrides. The TEM picture in Figure 1 showing δ-hydrides surrounded by γ-hydrides [35] in another zirconium alloy, Zr-2.5Nb, demonstrates that this interpretation has merit. Results of nano-beam electron diffraction experiments on Zircaloy-2 containing 1 at.% H have similarly been interpreted as δ-phase encased in γ-phase [28].

Neutron diffraction results also support the proposed composite hydride [33]. Areas of neutron diffraction peaks associated with γ-hydrides and δ-hydrides do not decrease monotonically with heating, but their sum does, following Equation 5 for C_-. This behaviour is expected if the γ-hydrides and δ-hydrides are not separate and independent, but are connected in a composite where their combined dissolution is constrained by an equilibrium relation. The neutron diffraction results suggest that the energetics of dissolution and precipitation of γ-hydrides and δ-hydrides are similar, otherwise the concentration of hydrogen in solution would change when, for example, γ-hydrides diminish and δ-hydrides increase in Zr-2.5Nb as they do on heating at 180 °C in Fig 8 of [33], but such a change in concentration of hydrogen in solution was not observed (see Fig. 4 of [33])[1]. The implication is that the heat required to dissolve the γ-hydrides is similar to the heat given off when the δ-hydride precipitates, on a per hydrogen atom basis. Density Functional Theory (DFT) that includes the effects of enthalpy as well as entropy and disorder concurs that γ-hydride and δ-hydride are very close in energy [4]. In the current study, no indication was observed in the DSC exothermic heat flow at 230 °C (Figure 3) where the γ-hydrides decline and δ-hydrides form in Figure 15. The extra exothermic heat flow that might be expected from the δ-hydride that forms after the γ-hydrides stop dissolving (Figure 16) would be small if the δ-hydride formed by condensation of hydrogen trapped in the surrounding hydrogen cloud containing the stoichiometric distribution of hydrogen.

[1] The temperature where γ-hydrides diminish and δ-hydrides increase on heating in [33] is similar to the temperatures where the ratio of C_+ to C_{TSS} for Zr-2.5Nb equals the stoichiometry ratios for Zr_4H_7 (1.75) and Zr_3H_5 (1.67): 180 °C and 210 °C, respectively.

Precipitates in metals that dissolve on cooling and form on heating: an example with hydrogen in alpha-zirconium

Figure 18 shows the phase diagram consistent with the interpretation of the current observations in which a boundary has been added at 0.5 mole fraction for ZrH γ-hydrides. Similar boundaries have been proposed previously [67, 69, 70]. If ZrH is a compound, then it is represented as a vertical line in the phase diagram. Figure 18 also shows a prediction of the boundary delineating the (γ+δ) phase field calculated from ratios of C_+ to C_{TSS} determined with Equation 6.

The diffraction line profile for δ-hydrides was not the same for formation and dissolution. When δ-hydrides formed the line grew symmetrically with time at 230 ^{o}C (Figure 15), but as the temperature was increased, successive isothermal measurements showed the line diminishing from left to right in Figure 10. The δ-hydride line profile includes contributions from δ-hydrides with reported stoichiometry from $ZrH_{1.5}$ to $ZrH_{1.67.}$ The d-spacings increase with stoichiometry as the lattice expands because of the extra hydrogen. The symmetric growth of the δ-hydride diffraction profile shown in Figure 15 suggests that the distribution of stoichiometry does not change when δ-hydrides condense from hydrogen trapped in hydrogen clouds formed when cooling. The range of stoichiometry depends on the range of C_+ values that exist when the δ-hydrides condense, which from the horizontal lines in Figure 8 should correspond to the temperature range of ≈35 ^{o}C, or from 230 ^{o}C to 230 ^{o}C + 35 ^{o}C for 1 at.% hydrogen. The corresponding ratios of C_+ to C_{TSS} are 1.6 to 1.7, which is the predicted range of stoichiometry for the condensing δ-hydrides. The width of the δ-hydride diffraction peak in Figure 15 includes this range of stoichiometry.

In contrast, when heated, the δ-hydride diffraction profile decays asymmetrically with the lowest stoichiometric hydrides systematically disappearing. Stable γ-hydride form with surrounding layers of hydrogen in solution trapped at concentrations C_+, C_{TSS} and C_-. When these layers condense to form δ-hydride, the concentration profile is recorded in the stoichiometry profile of the δ-hydride. When heated, the composite hydride dissolves systematically from the outermost layers.

Ab initio calculations suggest that the H-Zr stoichiometric ratio of γ-hydride could vary from 1.1 (0.52 mole fraction of H) at temperatures of 850 ^{o}C to 1.4 (0.58 mole fraction of H) at temperatures of 300 ^{o}C [70], in which case the vertical boundary line at 0.50 mole fraction (50 at.%) would be curved in Figure 18. The stoichiometry of the γ-hydride cannot be determined from the diffraction spectrum, it is assumed to be 1:1 as described in the Introduction. In the temperature range of this study, the position of the γ-hydride diffraction peak does not vary significantly suggesting any variation because of changes in stoichiometry is within the resolution of the measurement.

Comparison with previous interpretations

The temperatures in Figure 3 where exothermic and endothermic heat flows are most evident have been used to define two independent solvi: one for precipitation, and one for dissolution. On heating, the temperature at which the differential heat flow reaches a minimum value is sometimes called TSSD, which stands for terminal solid solubility at dissolution (315 ^{o}C in Figure 3). When the sample is cooled from the state where all of the hydrogen is in solution, the temperatures where exothermic changes can be observed start at 280 ^{o}C: this temperature is called the onset TSSP, where P stands for precipitation. The difference between the TSSD and TSSP solvi temperatures is now commonly called the 'hysteresis' [40]. A feature of the previous interpretation of the hysteresis is the hiatus inferred when switching between cooling and heating

where the concentration of hydrogen in solution does not change until TSSD is reached, as indicated by the horizontal line between Points C and D in Figure 2. This previous interpretation is not supported by the X-ray diffraction results because as soon as the temperature is increased, the lattice parameters of zirconium shown in Figure 14 rise monotonically indicating hydrogen going into solution.

The interpretation of the current results provides the underlying reasons for the apparent hysteresis. What has been called TSSP, is now labelled simply TSS, which is defined as the single solvus. The TSSD dissolution solvus of yore is C_-, which is determined directly from a J = 0 solution of the Einstein flux equation, and written in terms of the TSS concentration (Equation 5), which means TSSD is not an independent entity, and is not a solvus – it is the line about which the flux of hydrogen changes sign above the solvus temperature.

In the standard interpretation of TSS depicted in Figure 2, TSSP and TSSD concentrations exist at the same location, but at different times (when cooling and when heating, respectively, the concentrations are everywhere the same). In the current interpretation, the concentrations at equilibrium of hydrogen in solution associated with TSSP (TSS), and TSSD (C_-) exist at different locations at the same time.

Theoretical formulations have been developed, for example using accommodation energies required to form hydrides, to account for the apparent hysteresis, and to reconcile multiple solvi [39]; these formulations are unnecessary when invoking the Einstein flux equation.

Curiously, in Figure 9 hydrides were seen to form on cooling around 320 ^{o}C and might be inferred to dissolve finally on heating around 280 ^{o}C. These temperatures are reversed from the precipitation and dissolution temperatures determined from the DSC heat flow curves in Figure 3. If only δ-hydride peaks were observed, then it would appear that precipitation occurred at 230 ^{o}C and dissolution finally around 280 ^{o}C, which again is not in accord with the DSC heat flow curves in Figure 3. Diffraction data alone can be misleading without complementary information from DSC, which was used in this study to characterize the solvus by the onset precipitation temperature, or from other methods indicating hydride precipitation, for example dilatometry [40].

The apparent violation of the Phase Rule by simultaneous observation of hydrogen in solution and two hydride phases was resolved by containing the δ-phase within γ-phase at equilibrium. Previously, it was argued that the δ-phase and γ-phase could exist independently at the same time, but that the γ-phase is metastable and would not be present at equilibrium. Thus, the observation of γ-phase and δ-phase was interpreted to indicate these systems were not at equilibrium, which supported the 'restricted and dynamic' definitions of equilibrium during cooling and heating used to interpret TSSD and TSSP curves. The metastable argument requires that the γ-phase should eventually disappear, but it still persists after hours in our experiments and hours in neutron diffraction experiments with 0.783 at.% hydrogen in Zr-2.5Nb up to complete dissolution at 323 ^{o}C [33], and after three years at room temperature [11]. If γ-hydrides were consistently metastable, then heating should lead to their disappearance not just lead to reduced amounts [33]. The metastable argument is confounded by DSC experiments that show sharp reproducible indications of precipitation when cooling at rates of 5 ^{o}C to 30 ^{o}C per minute.

Precipitates in metals that dissolve on cooling and form on heating: an example with hydrogen in alpha-zirconium

The results of the current study suggest that γ-hydride is the equilibrium phase in contact with hydrogen in solution.

The formation of δ-phase requires some previous dissolution of γ-hydrides (e.g. see Figure 14 below T_- on cooling) to raise concentrations of hydrogen in solution to the values needed to form new hydrogen clouds when the δ-phase condenses (e.g. see Figures 13a and 14 at 230 ^{o}C). When the hydrogen trapped in clouds condenses to form δ-phase, the stabilizing hydrogen cloud is lost and a new cloud needs to form by taking hydrogen from the surrounding matrix to stabilize the newly condensed δ-phase. Thus, the prerequisite step for δ-hydride formation is for some γ-hydrides to dissolve partially, and then nucleate the δ-phase in the hydrogen cloud.

Nucleation of appropriate hydrides is the critical step to produce hydrides with their platelet normals parallel with a tensile stress leading to radial hydrides in tubes [71]. The athermal (γ^a) hydrides seen between 0^o and 20^o are forming close to the $\{10\bar{1}7\}$ hydride habit planes [72, 73], which are 14.7^o from the basal plane. If stabilized by applied tensile stress, these hydrides could act as the nucleation sites for damaging radial hydrides in pressure tubes with a strong transverse texture, similar to the current experimental material. The thermal (γ^t) hydrides are associated with the $\{10\bar{1}0\}$ habit planes [73] and are less likely to contribute to radial hydrides.

In the current study, hydrogen clouds were postulated to form in regions of tension to relieve the stress. Hydrogen clouds surrounding hydrides stunt their growth during cooling and stabilize them against dissolution during heating. During cooling, the stress-gradient regions, and not the hydrides, become sinks for hydrogen, and when satiated no more hydrogen flows. At equilibrium, the concentration at the unstressed hydride surface, which is C_{TSS}, and the concentration at the end of all the stress gradients must be the same, otherwise hydrogen would flow. Thus, at the point where the stress gradients go to zero, the conditions will be right for another hydride to nucleate, and a series of stable stunted hydrides are expected to form.

High-resolution micrographs of hydrides in zirconium alloys show that they are composed of linear arrays of small platelets [74], Figure 19. These ideas are reminiscent of θ' phase precipitation in Al-3 wt.% Cu. Precipitates of θ' phase originate at dislocations, but stop growing and then reinitiate via an autocatalytic nucleation process to form a linear array of plate-shaped precipitates. The resulting elastically-locked arrays are stabilized against growth or coarsening, or both [76].

DFT calculations of free energies for hydrides showed positive values for 1 at.% hydrogen in zirconium, which means that hydrides could not form; similar results were seen for hydrogen concentrations up to 2.7 at.% (300 ppm) [4], contrary to observations. This DFT free-energy calculation did not include the additional term to account for the work done to expand the solvent by the solute, which is the product of the hydrostatic pressure and the partial molar volume of the solute. This additional work term led to the drift term in Equation 3 and makes the free energies negative for hydride formation. Hydrides stabilized by a hydrogen cloud that forms in response to the misfit between the hydride and the matrix is consistent with suggestions from DFT that an additional hydrogen concentrating mechanism, such as “precipitate interface lattice strain”, is required to overcome the positive free energy calculated for hydride precipitation in zirconium with 1 at.% hydrogen [4].

The equations for C_+ and C_- should be generally applicable to any stress gradient within metals where a solute can move to relieve that stress gradient. The source of the stress gradient is decorated by a Cottrell atmosphere or a cloud of solute atoms until the limiting C_+ and C_- conditions are met, where the flux changes sign and the solute moves away from the stress source. The C_+ and C_- lines can be crossed by varying temperature and stress. Thus, an applied stress can be used to release the Cottrell atmosphere that prevents dislocations from moving, and maxima, called yield points, are seen in stress-strain curves [60]. Similarly, varying temperature was used in this work to unlock the Cottrell atmosphere or hydrogen cloud stabilizing hydrides against dissolution, and maxima were seen for the amounts of hydride formed with temperature.

We are aware that results presented in this paper run counter to common perceptions of what hydrides, and precipitates in general, are supposed to do when heated and cooled. But, think for a moment about the common perception that for hydrogen in zirconium there are two TSS solvus lines: one line applies when we cool, TSSP, and another line applies when we heat, TSSD (see Figure 2). The solvus defines an equilibrium condition, so it should not depend on direction of approach, yet the common perception is that it does for hydrogen in hydride forming metals, with zirconium being a clear example. What is counter to thermodynamics is equilibrium defined differently depending whether the system is heated or cooled. Over-all, we report that hydrides precipitate with cooling, and dissolve with heating, as expected. But, close to the solubility limit, because of the stress imposed by the hydrides on the lattice, we see these little perturbations. The flux of hydrogen to the hydrides depends on competing concentration gradients and stress gradients that orchestrate a marvelous dance about a central single solvus. The governing equation for this dance is of the form Einstein used to explain Brownian motion.

Concluding remarks

The behaviour of hydrides in zirconium have been observed using differential scanning calorimetry and X-ray diffraction on specimens of Zircaloy-2 containing up to 1 at.% hydrogen: hydrides both precipitate and dissolve on cooling and dissolve and precipitate on heating. These unexpected phenomena can be understood quantitatively with the Einstein flux equation, which is the sum of a concentration-gradient diffusion current (Fick's Law) and a drift current emanating from tensile stress gradients. Three zero-flux solutions to the equation exist. The solution where there are no gradients in concentration and stress defines the terminal solid solubility - the solvus. There are two solutions where the diffusion and drift currents are non-zero and cancel: these solutions define a region above and below the solvus where the flux of hydrogen is negative, and hydrides grow. Outside this region, the flux is positive and hydrides dissolve. The tensile stress can come from dislocations in the lattice, which can stabilize hydride formation above the solvus. The stress also comes from the edges around hydrides that put the local metal lattice into tension. Other sources of stress include differential thermal expansion leading to intergranular stresses. Hydrogen in solution moves into these tensile regions forming Cottrell atmospheres and hydrogen clouds to relieve the stress, which stabilizes the hydride against the effects of heating and cooling. One consequence of this interpretation is that hydrides should form linear arrays of small platelets. The lattice spacing of the zirconium matrix expands and contracts in response to the hydrogen going in and out of solution.

Precipitates in metals that dissolve on cooling and form on heating: an example with hydrogen in alpha-zirconium

It has not escaped our attention that this description of precipitation and particle dissolution should have general application to other hydride forming metals, for example Hf, Ti, Ta, Nb and V, and may be even more general for other precipitates.

Hydrides are inferred to form composite structures when δ-hydrides are observed. These composites will include a surrounding layer of γ-hydrides to satisfy the Phase Rule. There is no solvus for δ-hydrides; they are never at equilibrium with hydrogen in solid solution because there is always a γ-hydride intermediary.

Technological significances of these results are:

- Contrary to the usual interpretation, only a single terminal solid solubility limit (solvus) exists, based on precipitation of the γ-phase;

- The large differences inferred from DSC measurements (and other methods) between the temperatures at which hydrides start to precipitate and completely dissolve is not observed in these X-ray diffraction experiments. Hydrides have been observed to form on cooling at temperatures above the precipitation temperature inferred from DSC. The current results are useful for understanding phenomena such as delayed hydride cracking, blister formation, and hydride orientation;

- The δ-phase is not the equilibrium phase in contact with hydrogen in solution in the zirconium even when it is the most abundant phase. The implication of this conclusion is that the equilibrium phase diagram should include a boundary at 50 at.% (0.5 mole fraction) hydrogen. The observed stoichiometry of the δ-phase captured by the curvature of the γ+δ/δ line in the phase diagram can be calculated from the concentration of hydrogen in solution in hydrogen clouds that condense to form δ-hydrides;

- The temperature dependence of the precipitation process is complicated when compared with that of dissolution and contributes to the variation of hydride phases reported in the literature.

Precipitates in metals that dissolve on cooling and form on heating: an example with hydrogen in alpha-zirconium

Acknowledgements:

We would like to thank Argonne National Laboratory and J. Almer for setting up the X-ray source and diffraction equipment at the Advanced Photon Source, A. Buyers, C. Dixon, S. Hanlon, Z. He, B.W. Leitch, H. Nordin, S. Read, P. Wilson (all of CNL), C. Cochrane (Queen's U) and K. Colas (CEA) for help with the experiments, B. He (Carleton U.) for assistance with the analysis of the diffraction patterns. Useful discussions with J. Goldak and A. Artemev at Carleton University are much appreciated. CEC was supported as a Researcher Emeritus by CNL (né Atomic Energy of Canada Limited).

References

1. E. Zuzek, J.P. Abriata, A. San-Martin, F.D. Manchester, The H-Zr (Hydrogen-Zirconium) system, Bull. Alloy Phase Diagrams, 11 (1990) 385-395.
2. M. Christensen, W. Wolf, C. Freeman, E. Wimmer, R.B. Adamson, L. Hallstadius, P. Cantonwine, E.V. Mader, Effect of hydrogen on dimensional changes of zirconium and the influence of alloying elements: first-principles and classical simulations of point defects, dislocation loops and hydrides, Zirconium in the Nuclear Industry - Seventeenth International Symposium, ASTM STP 1543 (2014) 55-92.
3. C. Domain, R. Besson, A. Legris, Atomic-scale ab-initio study of the Zr-H system: I. Bulk properties, Acta Mater., 50 (2001) 3513-3526.
4. S.C. Lumley, S.T. Murphy, R.W. Grimes, M.R. Wenman, P.A. Burr, A. Chroneos, P.R. Chard-Tuckey, The thermodynamics of hydride precipitation: the importance of entropy, enthalpy and disorder, Acta Mat., 79 (2014) 351-362.
5. J.S. Bradbrook, G.W. Lorimer, N. Ridley, The precipitation of zirconium hydride in zirconium and Zircaloy-2, J. Nucl. Mater., 42 (1972) 142-160.
6. J.W. Gibbs, On the equilibrium of heterogeneous substances, Transactions of the Connecticut Academy, III., pp. 108–248, Oct. 1875–May, (1876), and pp. 343–524, May, 1877–July, (1878).
7. A. Einstein, Über die von der molekularkinetischen Theorie der Wärme geforderte Bewegung von in ruhenden Flüssigkeiten suspendierten Teilchen, Annalen der Physik, 322(8) (1905) 549–560.
8. G.A. McRae, C.E. Coleman, B.W. Leitch, The first step for delayed hydride cracking in zirconium alloys, J. Nucl. Mater., 396 (2010) 130-143.
9. J.E. Bailey, Electron microscope observations on the precipitation of zirconium hydride in zirconium, Acta Met., 11 (1963) 267-280.
10. C.D. Cann, A. Atrens, A metallographic study of the terminal solubility of hydrogen in zirconium at low hydrogen concentrations, J. Nucl. Mater., **88** (1980) 42-50.
11. S.S. Sidhu, N.S. Satya Murthy, F.P. Campos, D.D. Zauberis, Neutron and x-ray diffraction studies of nonstoichiometric metal hydrides, Advances Chem. Ser., **39** (1963) 87-98.
12. O.M. Katz, Tetragonal hydride in low hydrogen content Zircaloy, J. Nucl. Mater., **36** (1970) 335-339.
13. B. Nath, G.W. Lorimer, N. Ridley, Effect of hydrogen concentration and cooling rate on hydride precipitation in α-zirconium, J. Nucl. Mater., 58 (1975) 153-162.

14. C.D. Cann, M.P. Puls, E.E. Sexton, W.G. Hutchings, The effect of metallurgical factors on hydride phases in zirconium, J. Nucl. Mater., 126 (1984) 197-205.
15. J.K. Lee, Y.Y. Earmme, H.I. Aaronson, K.C. Russell, Plastic relaxation on the transformation strain energy of a misfitting spherical precipitate: ideal plastic behavior, Met.Trans., **11A** (1980) 1837-1847.
16. E. Tulk, M. Kerr, M.R. Daymond, Study on the effects of matrix yield strength on hydride phase stability in Zircaloy-2 and Zr-2.5 wt% Nb, J.Nucl. Mater., **425** (2012) 93-104.
17. D.O. Northwood, D.T.H. Lim, A TEM metallographic study of hydrides in a Zr-2.5 wt% Nb alloy, Metallography, **14** (1981) 21 – 35.
18. V. Perovic, G.C.Weatherly, The nucleation of hydrides in Zr-2.5 wt% Nb alloy, J. Nucl. Mater., **126** (1984) 160-169.
19. K.V. M. Krishna, D. Srivastava, G.K. Dey, V. Hiwarkar, and S. Banerjee, Role of grain/phase boundary nature on the formation of hydrides in Zr–2.5%Nb alloy, J. Nucl. Mater., **414** (2011) 270-275.
20. B. Nath, G.W. Lorimer, N. Ridley, The relationship between gamma and delta hydrides in zirconium-hydrogen alloys of low hydrogen concentration, J. Nucl. Mater., 49 (1973/74) 262-289.
21. L. Lanzani, M. Ruch, Comments on the stability of zirconium hydride phases in Zircaloy, J. Nucl. Mater., **324** (2004) 154-176.
22. M. Veleva, S. Arsene, M-C. Record, J.L. Bechade, J. Bai, Hydride embrittlement effects on the hoop mechanical properties of pressurized water reactor (PWR) and boiling water reactor (BWR) Zircaloy cladding tubes: Part II. Morphology of hydrides investigated at different magnifications and their interaction with the processes of plastic deformation, Met. Mat. Trans, **34A** (2003) 567-578.
23. R.S. Daum, Y.S. Chu, A.T. Motta, Identification and quantification of hydride phases in Zircaloy-4 cladding using synchrotron X-ray diffraction, J.Nucl. Mater., **392** (2009) 453-463.
24. S. Mishra, K.S. Sivaramakrishnan, M.K. Asundi, Formation of the gamma phase by a peritectoid reaction in the zirconium-hydrogen system, J. Nucl. Mater., **45** (1972/1973) 235-244.
25. K.G. Baraclough, C.J. Beevers, The nature of the γ-phase in zirconium-hydrogen alloys, J. Less-Common Mets., **35** (1974) 177-180.
26. K.G. Barraclough, C.J. Beevers, Some observations on the phase transformations in zirconium hydrides, J. Nucl. Mater., 34 (1970) 125-134.
27. K.E. Moore, Phase relationships in the α+δ region of the Zr-H system, J.Nucl. Mater., **32** (1969) 46-56.
28. A.T.W. Barrow, A. Korinek, M.R. Daymond, Evaluating zirconium-zirconium hydride interfacial strains by nano-beam electron diffraction, J. Nucl. Mater., 432 (2013) 366-370.
29. D.O. Northwood, Gamma and delta hydrides in zirconium alloys, J. Less-Common Mets., **48** (1976) 173-175.
30. K.B. Colas, A.T. Motta, J.D. Almer, M.R. Daymond, M. Kerr, A.D. Banchik, P. Vizcaino, and J.R. Santisteban, In-Situ study of hydride precipitation kinetics and re-orientation in Zircaloy using synchrotron radiation, Acta Mater., 58 (2010) 6575-6583
31. O. Zanellato, M. Preuss, J.-Y. Buffiere, F. Ribeiro, A. Steuwer, J. Desquines, J. Andreux, B. Krebs, Synchrotron diffraction study of dissolution and precipitation kinetics of hydrides in Zircaloy-4, J. Nucl. Mater., 420 (2012) 537-547;

Precipitates in metals that dissolve on cooling and form on heating: an example with hydrogen in alpha-zirconium

32. M.S. Blackmur, J.D. Robson, M. Preuss, O. Zanellato, R.J. Cernik, S.-Q. Shi, F. Ribeiro, J. Andrieux, Zirconium hydride precipitation kinetics in Zircaloy-4 observed with synchrotron X-ray diffraction, J. Nucl., Mater., 464 (2015) 160-169.
33. J.H. Root, R.W.L. Fong, Neutron diffraction study of the precipitation and dissolution of hydrides in Zr-2.5 Nb pressure tube material, J. Nucl. Mat., **232** (1996) 75-85.
34. W.M. Small, J.H. Root, D. Khatamian, Observation of kinetics of γ zirconium hydride formation in Zr-2.5Nb by neutron diffraction, J. Nucl. Mat., **256** (1998) 102- 107.
35. J.H. Root, W.M. Small, D. Khatamian, O.T.Woo, Kinetics of the δ to γ zirconium hydride transformation in Zr-2.5 Nb, Acta Mat., 51 (2003) 2041-2053.
36. M. Christensen, W. Wolf, C. Freeman, E.Wimmer, R.B. Adamson, L. Hallstadius, P. Cantonwine, E.V. Mader, Effect of hydrogen on dimensional changes of zirconium and the influence of alloying elements: first-principles and classical simulations of point defects, dislocation loops and hydrides, Zirconium in the Nuclear Industry- Seventeenth International Symposium, ASTM STP 1543, (2014), 55-92.
37. C. Domain, R. Besson, A. Legris, Atomic-scale ab-initio study of the Zr H system: I. Bulk properties, Acta Mater., 50 (2002) 3513-3526.
38. International Atomic Energy Agency, Delayed hydride cracking in zirconium alloys in pressure tube nuclear reactors, IAEA-TECDOC-1410, (2004)
39. M.P. Puls, The effects of hydrogen and hydrides on the integrity of zirconium alloy components – delayed hydride cracking, Engineering Materials, (Springer-Verlag, London, 2012).
40. W.H. Erickson, D. Hardie, The influence of alloying elements on the terminal solubility of hydrogen in α-zirconium, J. Nucl. Mater., 13 (1964) 254-262.
41. J.J. Kearns, Thermal expansion and preferred orientation in Zircaloy, WAPD-TM-472 (1965).
42. Anonymous, Standard test methods for tension testing of metallic materials, ASTM International, E8/E8M-15 (Approved 2015).
43. Anonymous, Standard test methods for elevated temperature tension tests of metallic materials, ASTM International, E21-09 (Approved 2009).
44. G.A. Bickel, L.W. Green, M.W.D. James, T.G. Lamarche, P.K. Leeson, H. Michel, "The Determination of Hydrogen and Deuterium in Zr–2.5Nb Material by Hot Vacuum Extraction Mass Spectrometry", Journal of Nuclear Materials 306, 2002, p. 21.
45. K. Colas, A. Motta, M.R. Daymond, J. Almer, "Mechanisms of Hydride Reorientation in Zircaloy-4 Studied in Situ," Zirconium in the Nuclear Industry: 17th International Symposium, STP 1543, Robert Comstock and Pierre Barberis, Eds., pp. 1107–1137, doi:10.1520/STP154320120168, ASTM International, West Conshohocken, PA 2015
46. J. Goldak. Lattice Parameters, Thermal Expansions, and Grüneisen Coefficients of Zirconium, 4.2 to 1130 _K, Physical Review, 144(2) (1966) 478-484.
47. S.R. MacEwen, C.E. Coleman, C.E. Ells, J. Faber Jr, Dilation of HCP Zirconium by Interstitial Deuterium, Acta Metall. 33 (1985) 753-757.
48. E. Zuzek, J.P. Abriata, A. San-Martin, F.D. Manchester, The H-Zr (Hydrogen-Zirconium) system, Bull. Alloy Phase Diagrams, 11 (1990) 385-395.
49. I. Ferguson, United Kingdom Atomic Energy Assoc.-TRG Report, v2438 p1 (1976)
50. S.S. Sidhu, N.S. Satya Murthy, F.P. Campos, D.D. Zauberis, Adv. Chem. Ser., 39 (1963) p87.

1172 51. G.J.C. Carpenter, The dilatational misfit of zirconium hydrides precipitated in zirconium, J.
1173 Nucl. Mater., 48 (1973) 264-266.
1174 52. R.N. Singh, P. Ståhle, A.R. Massih, A.A. Shmakov, Temperature dependence of misfit
1175 strains of δ-hydrides of zirconium, J. Alloys Cmpd., 436 (2007) 150-154.
1176 53. B.D. Cullity, Elements of X-ray Diffraction, 2nd Ed., Appendix 3, Addison-Wesley Co, 1978.
1177 54. International Union of Pure and Applied Chemistry (1993). Quantities, Units and Symbols in
1178 Physical Chemistry, 2nd edition, Oxford: Blackwell Science. ISBN 0-632-03583-8. pp. 49–
1179 50
1180 55. A. Fick, On liquid diffusion, Phil. Mag., 10, 30-39 (1855).
1181 56. J.R. Rice, G.F. Rosengren, Plane strain deformation near a crack in a power law hardening
1182 material, J. Mech. Phys. Solids, 16 (1968) 1-12.
1183 57. J.W. Hutchinson, Singular behaviour at the end of a tensile crack in a hardening material, J.
1184 Mech. Phys. Solids, 16 (1968) 13-31.
1185 58. M.F. Kanninen, C.H. Popelar, Advanced Fracture Mechanics, Oxford University Press
1186 (1985).
1187 59. K. Hellan, Introduction to Fracture Mechanics, McGraw-Hill, New York (1985).
1188 60. A.H. Cottrell, Effect of solute atoms on the behaviour of dislocations, Report of a Conf. on
1189 Strength of Solids, Univ. of Bristol, July 7-9 (1947).
1190 61. A. McMinn, E.C. Darby, J.S. Schofield, The terminal solid solubility of hydrogen in
1191 zirconium alloys, Zirconium in the Nuclear Industry - Twelfth International Symposium,
1192 ASTM STP 1354 (2000) 173-195.
1193 62. R.L. Eadie, K. Tashiro, D. Harrington, M. Leger, The determination of the partial molar
1194 volume of hydrogen in zirconium in a simple stress gradient using comparative
1195 microcalorimetry, Scripta Met. Mat., 26, (1992), 231-236.
1196 63. B.W. Leitch, S. St.Lawrence, Stress-triaxiality in Zr-2.5Nb pressure tube materials, J. ASTM
1197 Int. 6(2) (2009) 1-13.
1198 64. Z.L. Pan, I,G. Ritchie, M.P. Puls, The terminal solid solubility of hydrogen and deuterium in
1199 Zr-2.5Nb alloys, J. Nucl. Mater., 228 (1996), 227-237.
1200 65. W. Ostwalt, "Studien über die Bildung und Umwandlung fester Körper" [Studies on the
1201 formation and transformation of solid bodies], Zeitschrift für physikalische Chemie. 22
1202 (1897) 289–330.
1203 66. E. Königsberger, G. Eriksson, W.A. Oates, Optimisation of the thermodynamic properties of
1204 the Ti-H and Zr-H systems, J. Alloys Cmpds, 288 (2000) 148-152.
1205 67. S. Mishra, K.S. Sivaramakrishnan and M.K. Asundi, Formation of the gamma phase by a
1206 peritectoid reaction in the zirconium-hydrogen system, J. Nucl. Mater., 45 (1972/73) 235-
1207 244.
1208 68. Y.V. Levinskii, R.A. Andriyevskiy, and E.B. Boyko, The pressure-temperature and
1209 temperature-composition diagrams for the zirconium-hydrogen system, Russ. Metall., (1975)
1210 151-154.
1211 69. A.M. Solodinin, E.B. Boyko, and R.A. Andriyevskiy, Autoradiographic and metallographic
1212 study of the γ-phase in the Zr-H system, Russ. Metall., (1978) 178-183.
1213 70. M. Christensen, W. Wolf, C. Freeman, E.Wimmer, R.B. Adamson, L. Hallstadius, P.
1214 Cantonwine, E.V. Mader, H in α-Zr and in zirconium hydrides: solubility, effect on
1215 dimensional changes, and the role of defects, J. Phys.: Condens. Matter 27 (2015) 12pp.
1216 71. C.E. Ells, The stress orientation of hydrides in zirconium alloys, J. Nucl. Mater., 35 (1970)
1217 306-315

1218 72. D.G. Westlake, The habit planes of zirconium hydride in zirconium and Zircaloy, J. Nucl.
1219 Mater., 26, (1968) 208-216.
1220 73. G.C. Weatherly, The precipitation of γ-hydride plates in zirconium, Acta Mater., 29, (1981)
1221 501-512
1222 74. G.W. Parry, Stress reorientation of hydrides in cold-worked zirconium-2.5% niobium
1223 pressure tubes, Atomic Energy of Canada Ltd, AECL 2624 (1966).
1224 75. H. Nordin, (Canadian Nuclear Laboratories) private communication (2017).
1225 76. V. Perovic, G.R. Purdy, L.M. Brown, Autocatalytic nucleation and elastic stabilization of
1226 linear arrays of plate-shaped precipitates, Acta Met. 29 (1981) 889-902.

1227

Precipitates in metals that dissolve on cooling and form on heating: an example with hydrogen in alpha-zirconium

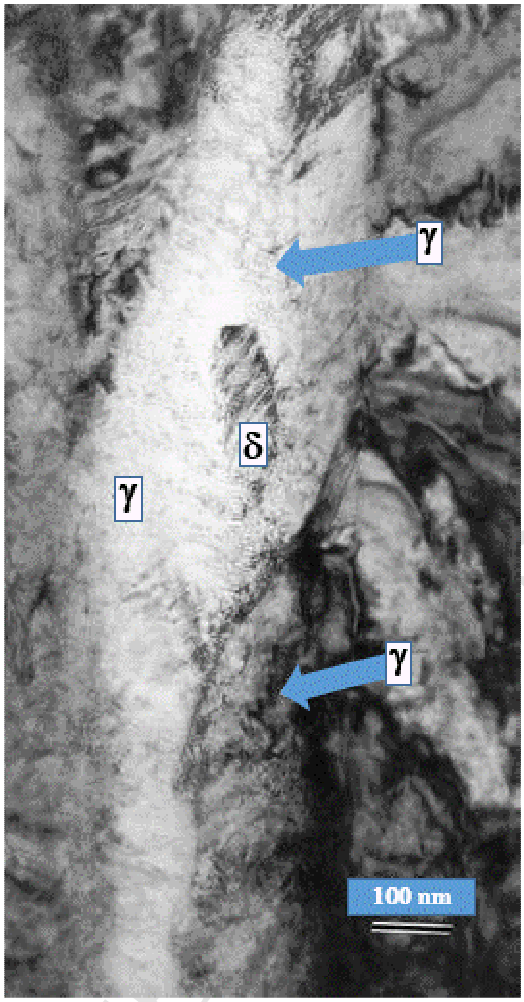

Figure 1: TEM micrograph showing δ-hydride surrounded by γ-hydride in Zr-2.5Nb, based on [35].

Precipitates in metals that dissolve on cooling and form on heating: an example with hydrogen in alpha-zirconium

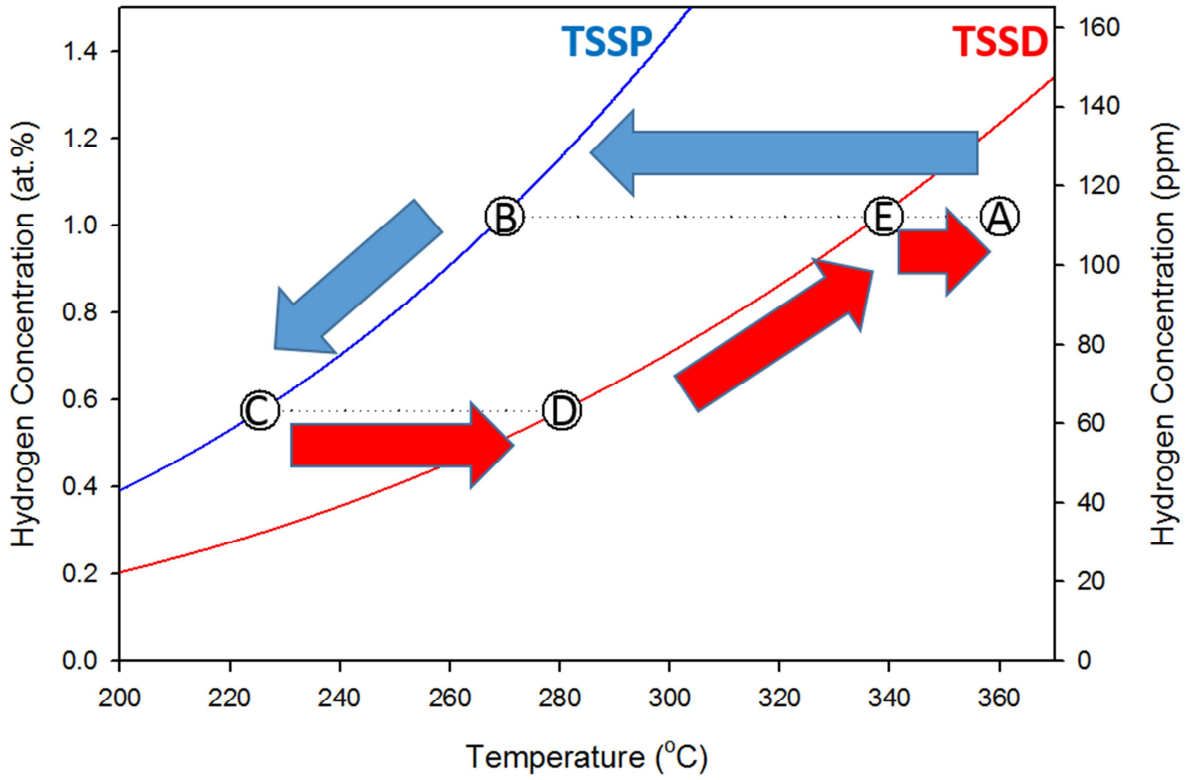

Figure 2: TSS lines for 1 at.% hydrogen in Zircaloy-2 and some points that are used in the text to illustrate the standard interpretation of a cooling-heating cycle starting at Point A and proceeding to Points B-C-D-E and back to A.

Precipitates in metals that dissolve on cooling and form on heating: an example with hydrogen in alpha-zirconium

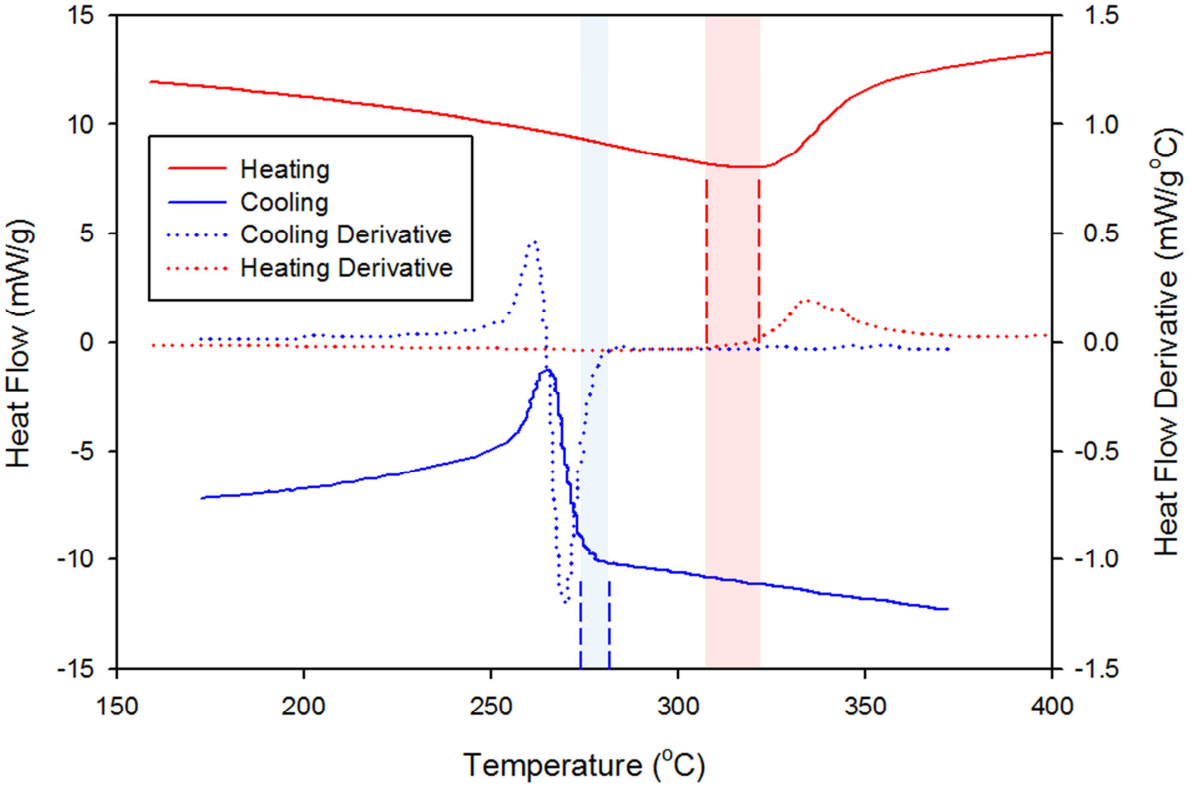

Figure 3: DSC heating and cooling curves for 1 at.%, (113±4) ppm, hydrogen in zirconium. The vertical coloured bands show one standard deviation about the mean of measurements of the onset temperature for precipitation on cooling, the TSS or solvus (278 °C ± 4 °C; left band; blue), and the minimum heat-flow temperature on heating (T_+ = 315 °C ± 7 °C; right band; pink).

1235

1236

1237

1238

Precipitates in metals that dissolve on cooling and form on heating: an example with hydrogen in alpha-zirconium

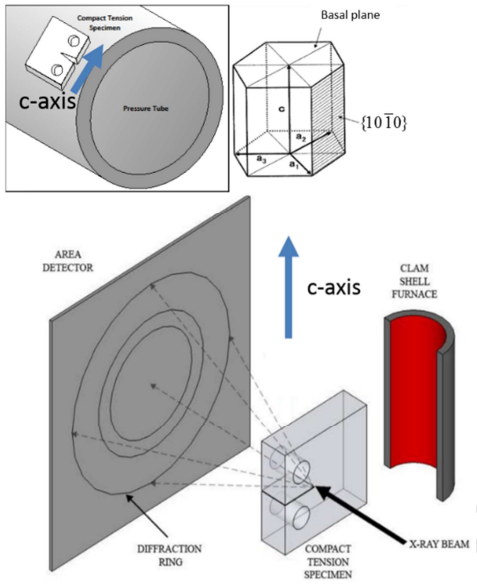

Figure 4: Experimental arrangement (not to scale).

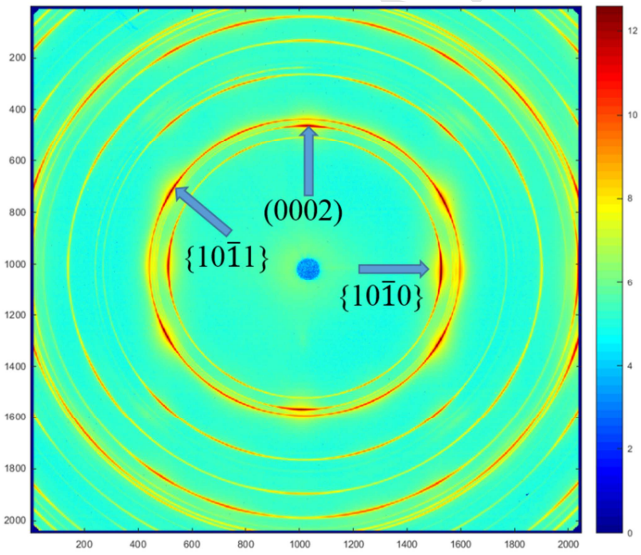

Figure 5: Diffraction rings from the Zircaloy-2 specimen with hydrogen concentration 0.1 at.%, (12±3) ppm. The intensity scale is arbitrary. The innermost most ring is {10$\bar{1}$0}, the next ring is (0002). The variable intensity around the circumference of each ring is because of the texture in the zirconium: the basal plane normals tend to point 'north', or towards 12 o'clock, because of the predominant transverse texture of the pressure tube from which the specimens were cut. The zirconium specimens were cut in the form of compact toughness specimens, but the notch was not examined in this experiment: all reported observations were made at distances of millimeters from the notch, which was loaded with 10 N to hold the specimens in place.

Precipitates in metals that dissolve on cooling and form on heating: an example with hydrogen in alpha-zirconium

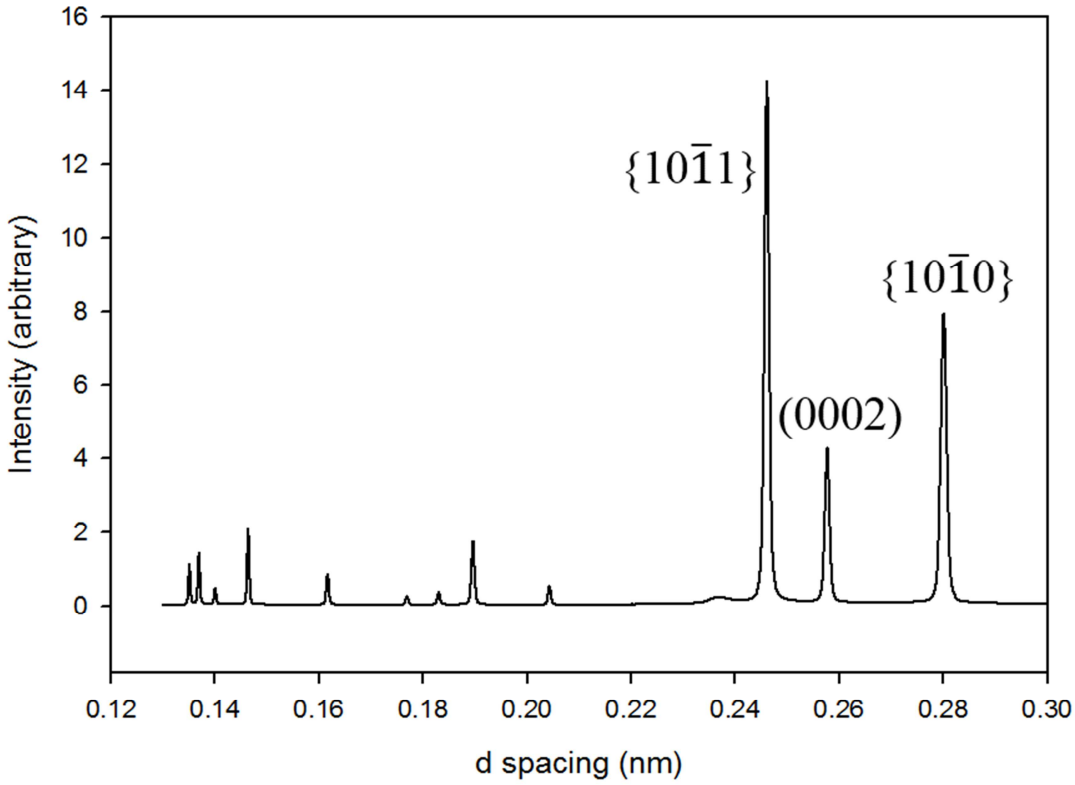

Figure 6: Diffraction spectrum of the Zircaloy-2 specimen with hydrogen concentration 0.1 at.%, (12±3) ppm. The basal (0002) plane, prism plane {10$\bar{1}$0}, and pyramidal {10$\bar{1}$1} diffraction lines are labeled. This spectrum is the sum of spectra from 14 different locations in the specimen.

Precipitates in metals that dissolve on cooling and form on heating: an example with hydrogen in alpha-zirconium

1258

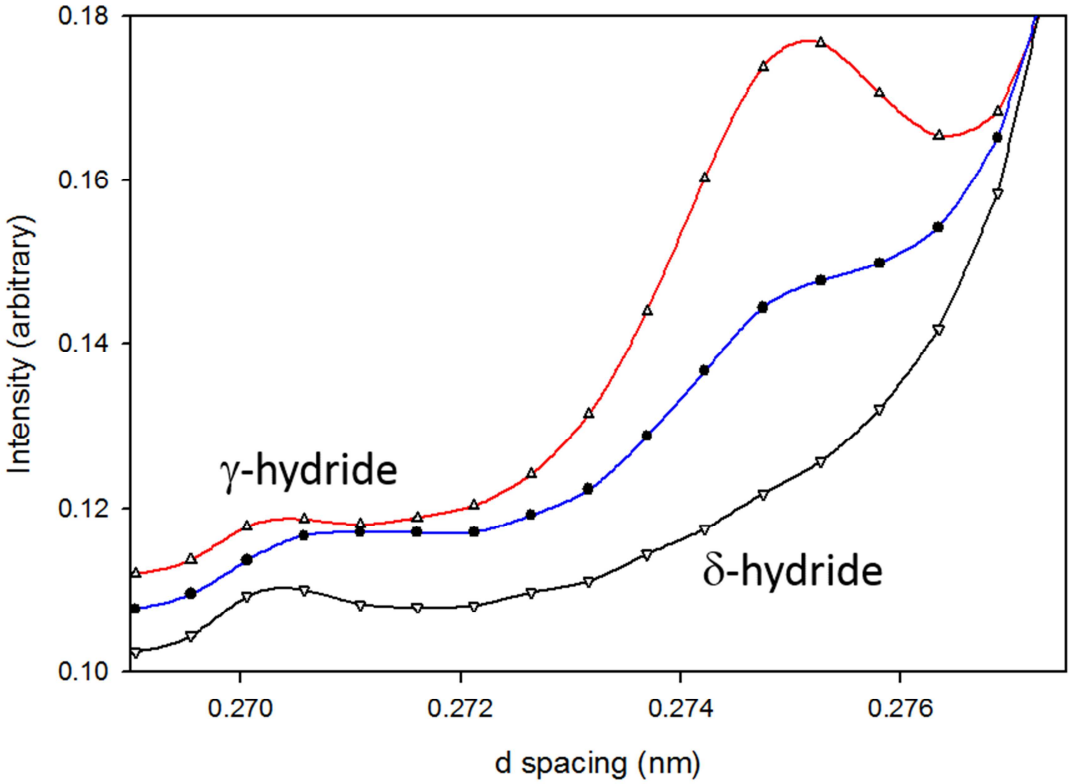

1259

1260 Figure 7: Diffraction lines in the region where peaks associated with diffraction from {111}
1261 planes of γ- and δ-hydrides can be found for three hydrogen concentrations (1, 0.6 and 0.1 at.%,
1262 (113±4, 63±4, and 12±3) ppm, top to bottom) at room temperature after cooling (summed from
1263 14 separate locations in each specimen). The spectra are successively offset by 0.005 intensity
1264 units from the low concentration spectrum. The γ-hydride signal is relatively constant compared
1265 with the δ-hydride signals, which are larger for larger hydrogen concentrations. Only γ-hydrides
1266 are seen for the specimen containing a low concentration of hydrogen.

1267

Precipitates in metals that dissolve on cooling and form on heating: an example with hydrogen in alpha-zirconium

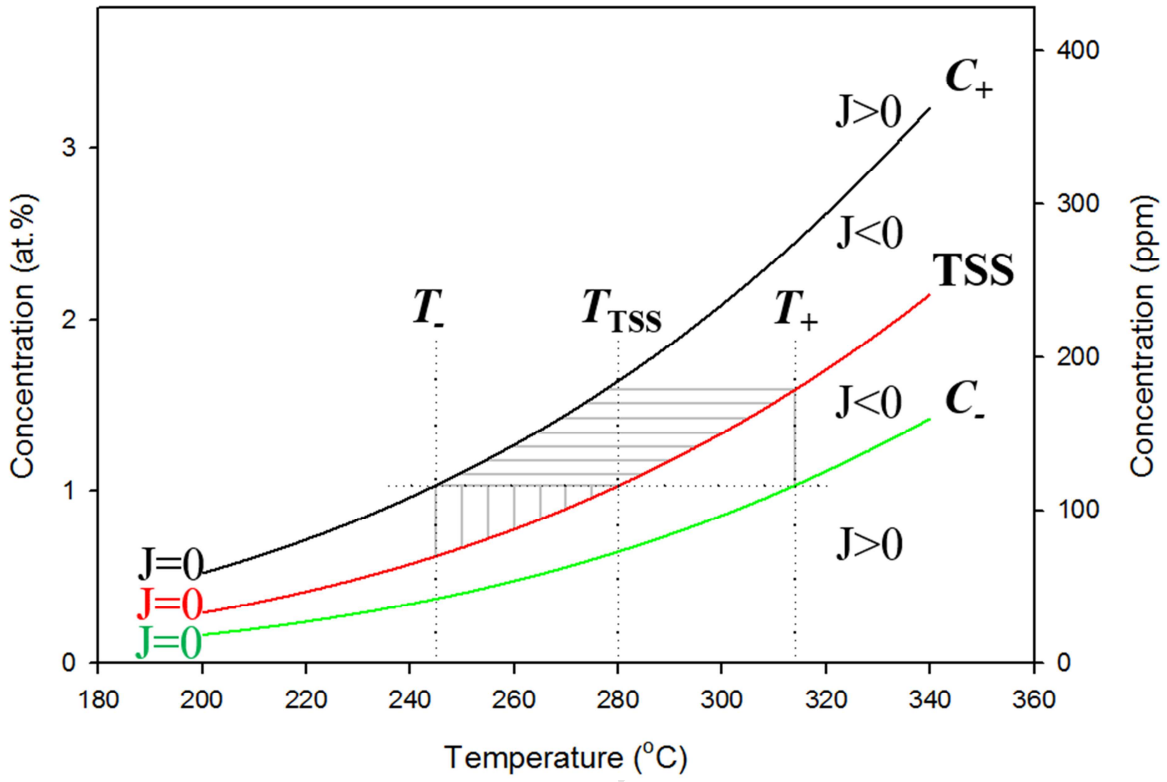

Figure 8: The no-flux solutions to the Einstein flux equation when hydrides are present (C_+, TSS, C_-); in the regions between these three solutions the initial flux of hydrogen in solution, J, is negative and hydrogen flows towards regions of tensile stress forming hydrides. Vertical dotted lines show the upper and lower 'J < 0' temperature limits calculated with $K = 2$. The solvus is at 280 °C for 1 at.% hydrogen, which is shown by the horizontal dotted line. The solid vertical and horizontal lines are used to describe γ^a-hydride precipitation and dissolution above and below the solvus temperature, as detailed in the text.

Precipitates in metals that dissolve on cooling and form on heating: an example with hydrogen in alpha-zirconium

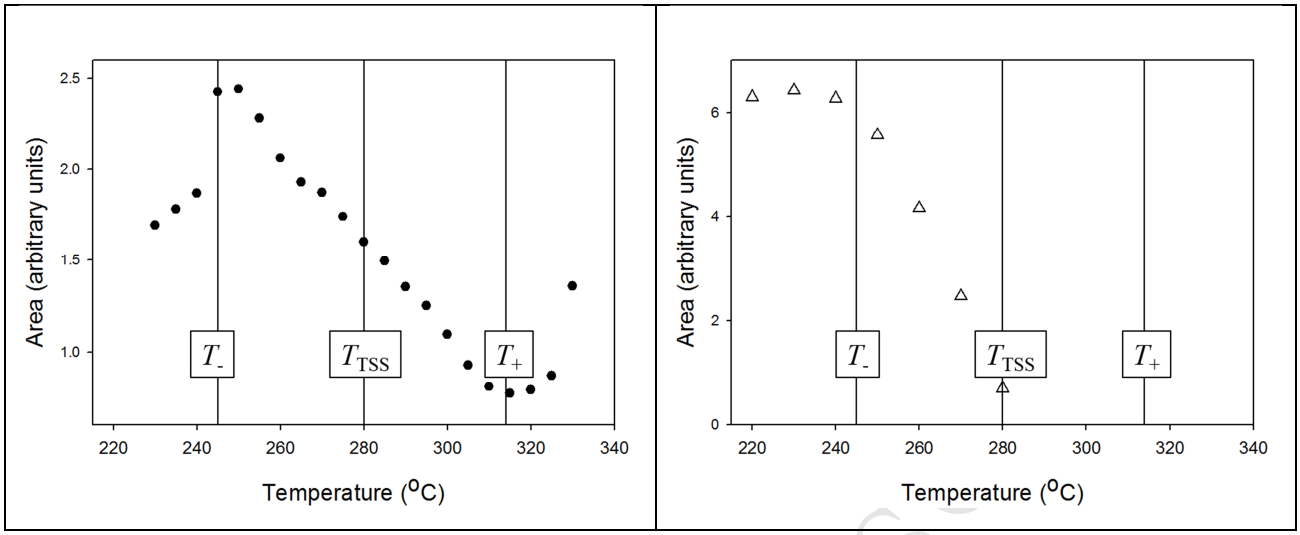

Figure 9: Areas of {111} hydride diffraction peaks integrated around the diffraction rings for the specimen with 1 at.%, (113±4) ppm, hydrogen: γ-hydrides on cooling (left) and δ-hydrides on heating (right). The vertical lines show T_-, the solvus temperature, and T_+ for $K = 2$, as discussed in the text.

Precipitates in metals that dissolve on cooling and form on heating: an example with hydrogen in alpha-zirconium

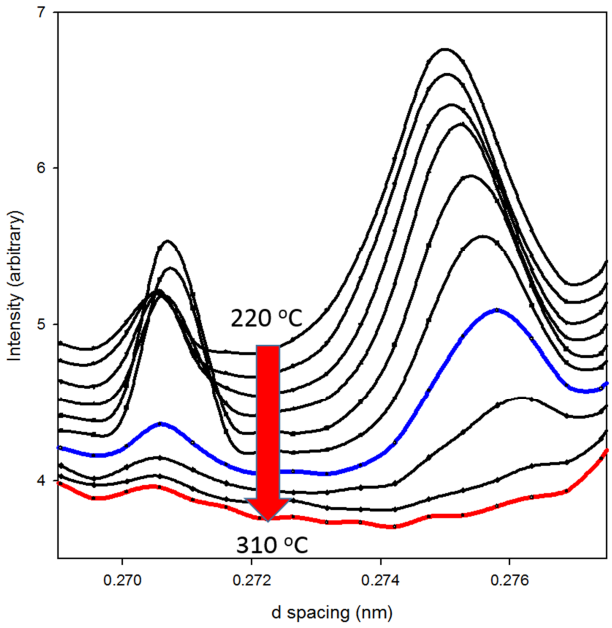

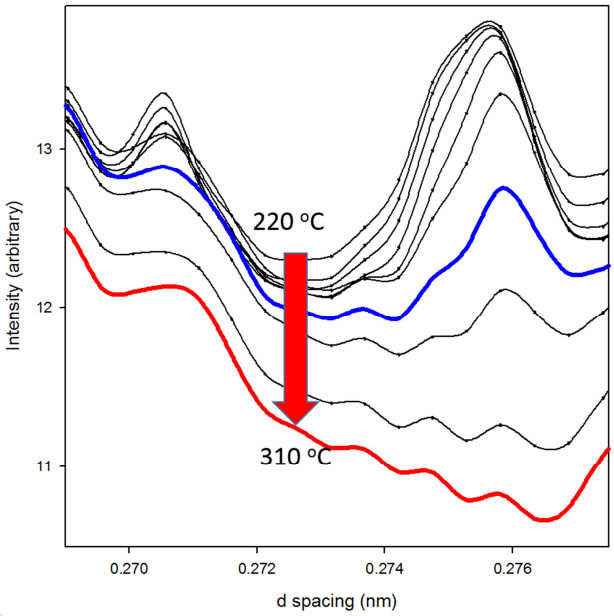

Figure 10: Spectra obtained with 1 at.%, (113±4) ppm, H in Zircaloy-2 for a series of isothermal measurements obtained by integrating intensity around the diffraction ring from 55° to 75° (top) and 0° to 20° (bottom). The temperature of the spectrum drawn in blue is the same as the onset precipitation temperature determined from DSC (278 °C ± 4 °C); the temperature of the red-coloured spectrum is similar to the minimum heat-flow temperature during heating (315 °C ± 7 °C).

Precipitates in metals that dissolve on cooling and form on heating: an example with hydrogen in alpha-zirconium

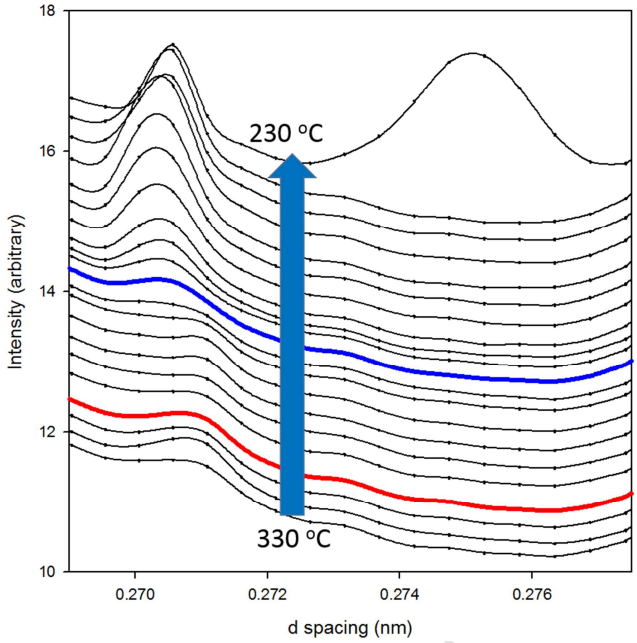

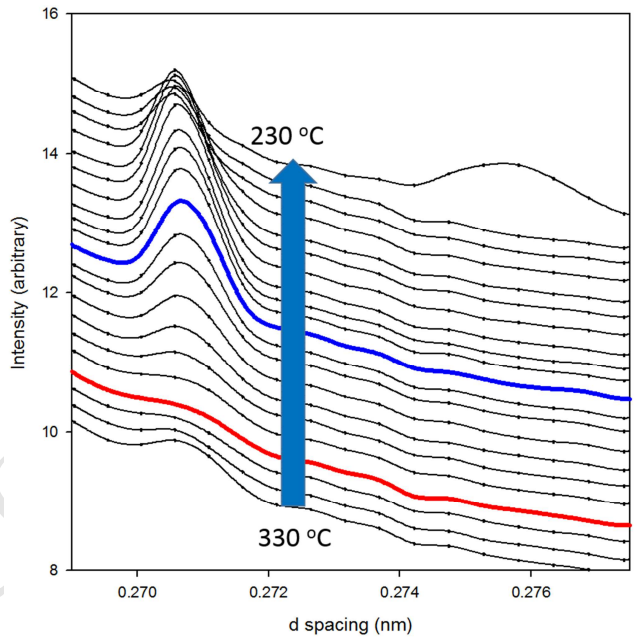

Figure 11: Spectra obtained with 1 at.%, (113±4) ppm, H in Zircaloy-2 for a series of isothermal measurements obtained by integrating intensity around the diffraction ring from 55° to 75° (top) and 0° to 20° (bottom). The temperature of the spectrum drawn in blue is the same as the onset precipitation temperature determined from DSC (278 °C ± 4 °C); the temperature of the red-coloured spectrum is similar to the minimum heat-flow temperature during heating (315 °C ± 7 °C).

Precipitates in metals that dissolve on cooling and form on heating: an example with hydrogen in alpha-zirconium

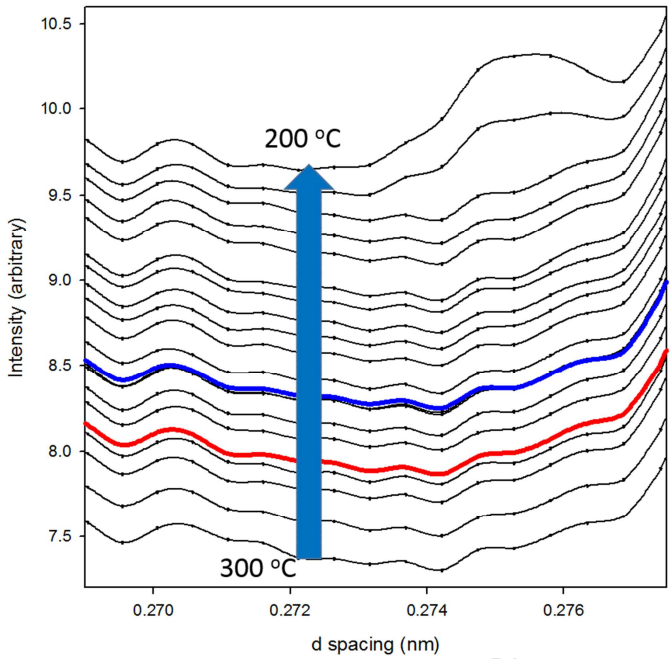

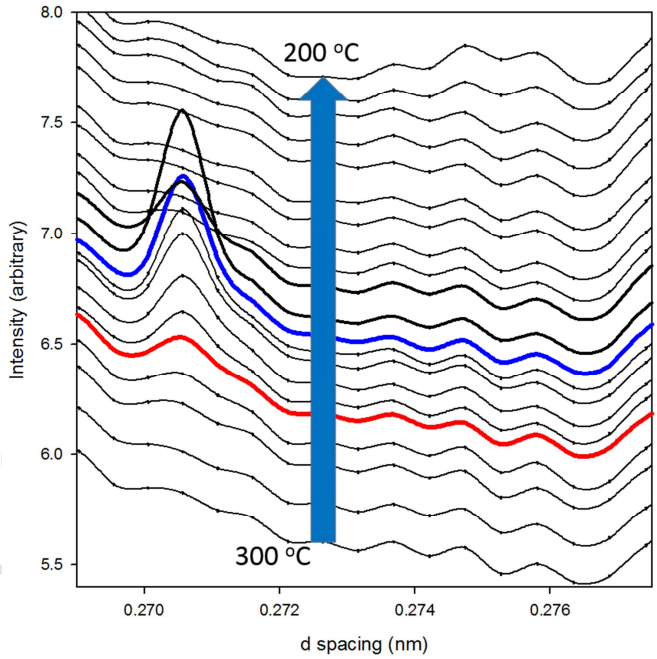

Figure 12: Spectra obtained with 0.6 at.%, (63±4) ppm, H in Zircaloy-2 for a series of isothermal measurements obtained by integrating intensity around the diffraction ring from 55° to 75° (top) and 0° to 20° (bottom). The temperature of the spectrum drawn in blue is the same as the onset precipitation temperature determined from DSC (255.3 °C ± 2 °C); the temperature of the red-

1305 coloured spectrum is similar to the minimum heat-flow temperature during heating (282.4 °C ±
1306 2 °C).

1307

Precipitates in metals that dissolve on cooling and form on heating: an example with hydrogen in alpha-zirconium

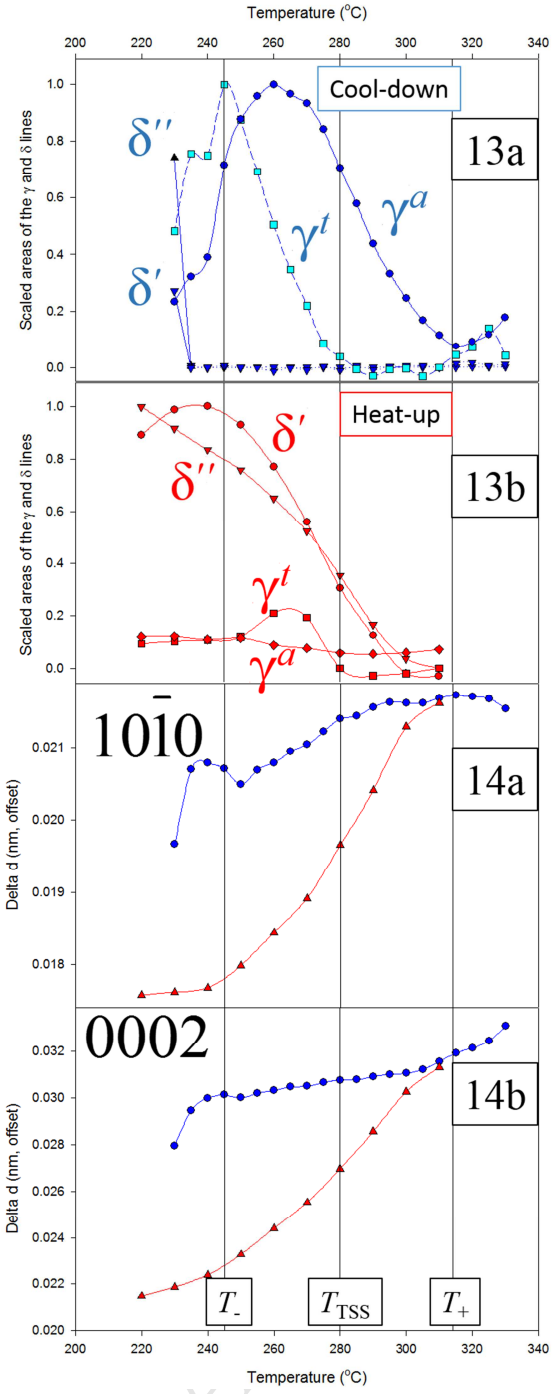

Figure 13: Normalized areas of hydride diffraction peaks obtained during cooling (a) and heating (b): δ″-hydrides and γ^t-hydrides are seen between 55° and 75° around the ring; δ′-hydrides and γ^a-hydrides are seen between 0° and 20°. The vertical lines show, left to right, T_-, the solvus temperature, and T_+ for K=2, as discussed in the text. (1 at.%, (113±4) ppm, H in Zircaloy-2)

Figure 14: d-spacings for the {10$\bar{1}$0} (a) and (0002) (b) α-zirconium lines, determined by integrating around the diffraction ring, and corrected for thermal expansion. Values of 'Delta d' are proportional to the concentration of hydrogen in solid solution. Circles denote cool-down and triangles heat-up. (1 at.%, (113±4) ppm, H in Zircaloy-2)

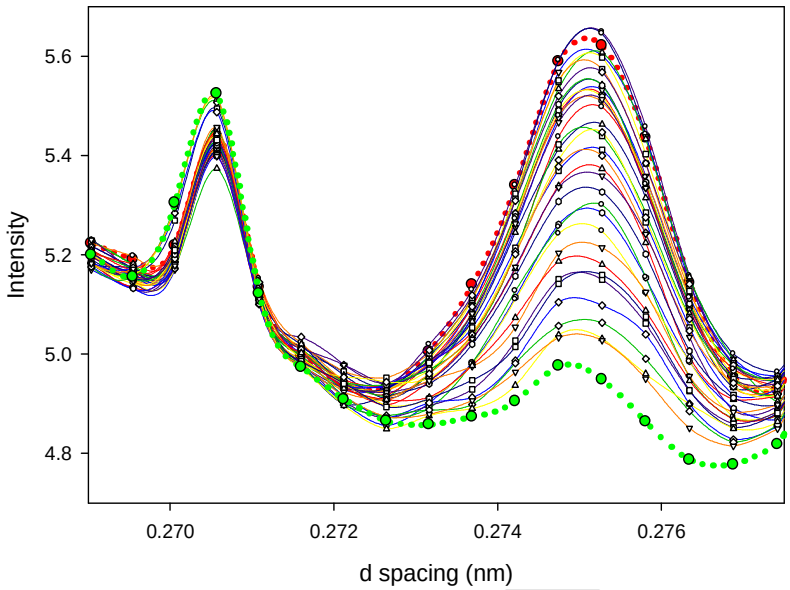

Figure 15: Diffraction peaks from {111} planes of the γ^t-hydrides (left) and δ''-hydrides (right) at 0.5 s intervals after cooling from 235 ^{o}C to 230 ^{o}C, at 10 ^{o}C/min, and a 3 min isothermal hold. The first spectrum in the time sequence is shown by green-filled circles connected with green dots; the last spectrum is red-filled circles connected by red dots. The areas of the peaks as a function of time are shown in Figure 16. The intensities of the peaks were measured around the diffraction ring from 55^{o} to 75^{o}. (1 at.%, (113±4) ppm, H in Zircaloy-2)

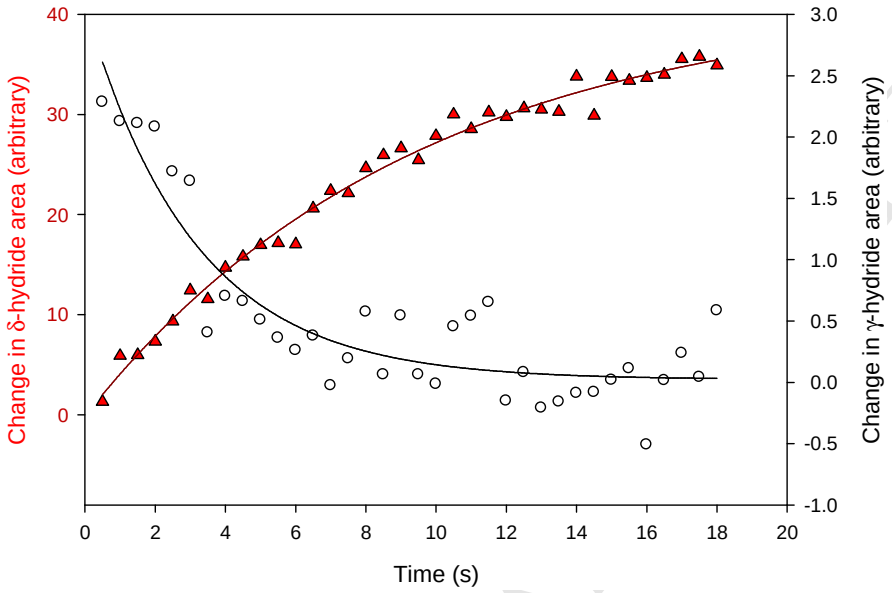

Figure 16: Time dependence of the areas of the diffraction peaks shown in Figure 15 from {111} planes of the γ-hydrides and δ-hydrides starting 3 min after cooling from 235 ^{o}C to 230 ^{o}C at 10 ^{o}C/min. The γ-hydride peak areas decrease in the first few seconds, then stop. The δ-hydride peaks continually increase over the observation time of 18 s. The zirconium diffraction peaks did not move over this time. The hydride areas are relative to the initial and final areas of the δ- and γ-hydride peaks, respectively.

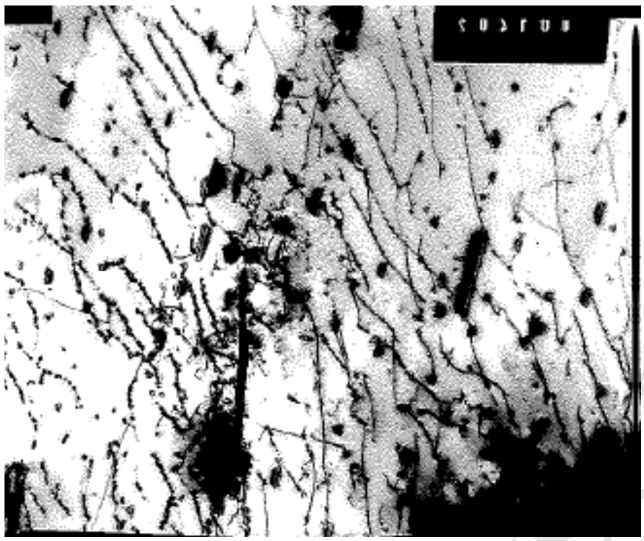

Figure 17: Thin-film transmission electron micrograph of Zircaloy-2 specimen showing dislocation lines decorated with hydride particles.

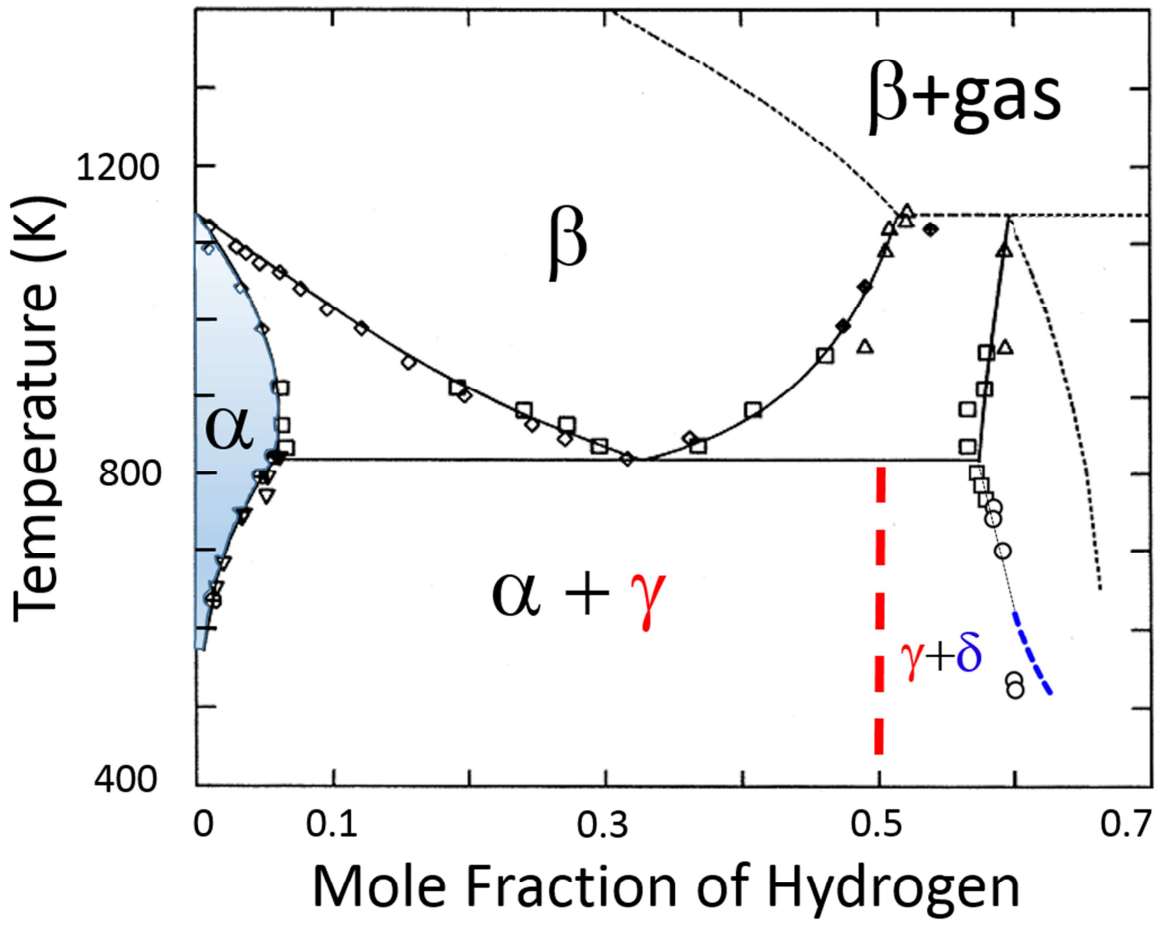

Figure 18: Zirconium-Hydrogen phase diagram based on [66]. The dashed vertical line for 0.5 mole fraction is proposed for γ-hydride (ZrH). The solvus is the equilibrium boundary that separates the shaded region (α), where hydrogen is in solid solution in the α-zirconium matrix, and the region (α + γ-hydride), where ZrH hydrides have precipitated in the matrix. Mole fractions about 0.6 are associated with δ-hydrides. The dashed blue curve is the γ+δ/δ boundary calculated from concentrations of hydrogen in solution in hydrogen clouds that condense to form δ-hydrides (Equation 6). For mole fractions between 0.5 and 0.6, γ-hydride is in equilibrium with δ-hydride. The simultaneous observation of γ-hydrides and δ-hydrides apparently in equilibrium with hydrogen in solution suggests that to satisfy Gibbs' Phase Rule δ-hydrides are surrounded by a layer of γ-hydride.

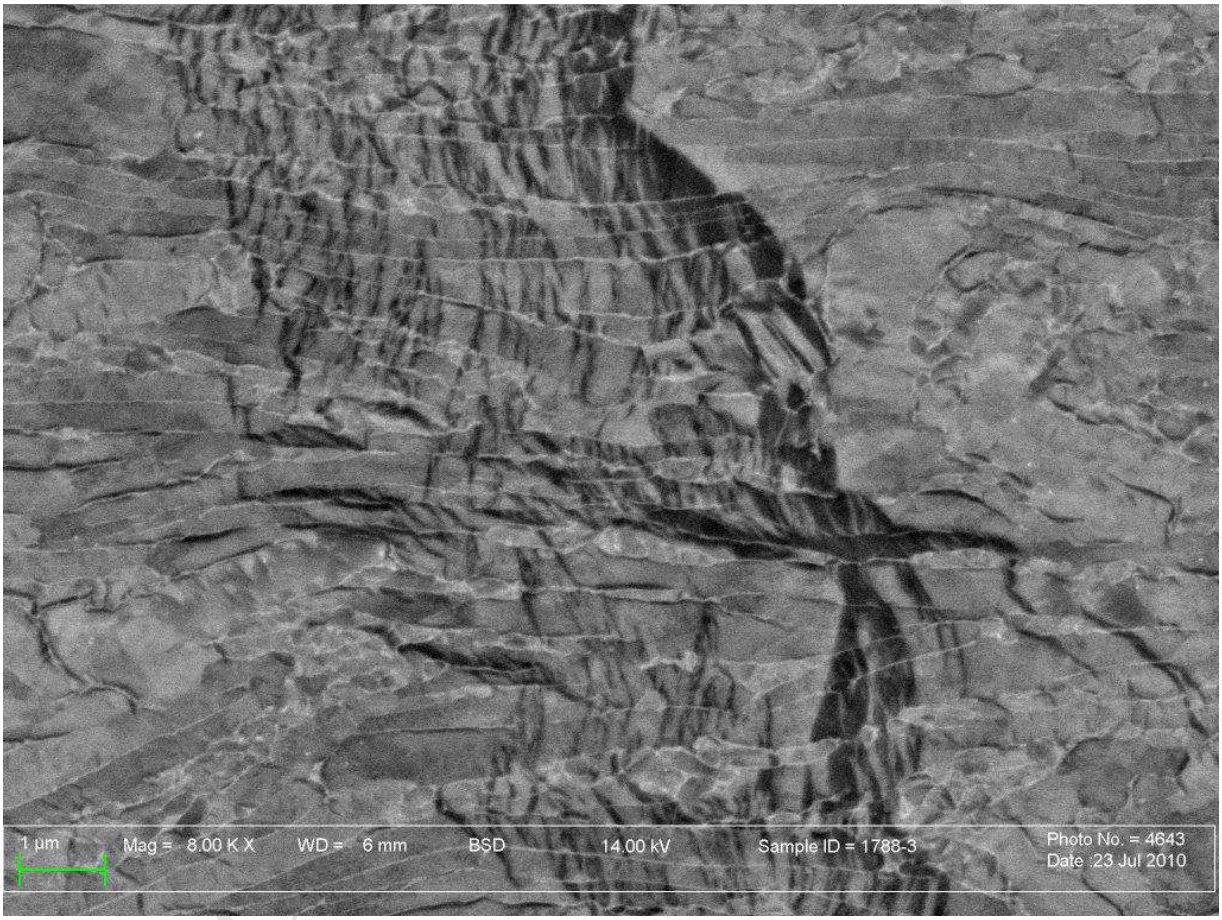

Figure 19: Electron-backscatter SEM micrograph showing ‘black’ hydride platelets forming linear arrays in Zr-2.5Nb [75]. At lower magnification in light microscopy, these platelets appear as single particles.